

This is a repository copy of *A multi-omics approach to lignocellulolytic enzyme discovery reveals a new ligninase activity from Parascedosporium putredinis NO1*.

White Rose Research Online URL for this paper:

<https://eprints.whiterose.ac.uk/173215/>

Version: Accepted Version

---

**Article:**

Oates, Nicola Claire, Abood, Amira, Schirmacher, Alexandra et al. (11 more authors) (2021) A multi-omics approach to lignocellulolytic enzyme discovery reveals a new ligninase activity from *Parascedosporium putredinis* NO1. Proceedings of the National Academy of Sciences of the United States of America. e2008888118. ISSN 1091-6490

<https://doi.org/10.1073/pnas.2008888118>

---

**Reuse**

Items deposited in White Rose Research Online are protected by copyright, with all rights reserved unless indicated otherwise. They may be downloaded and/or printed for private study, or other acts as permitted by national copyright laws. The publisher or other rights holders may allow further reproduction and re-use of the full text version. This is indicated by the licence information on the White Rose Research Online record for the item.

**Takedown**

If you consider content in White Rose Research Online to be in breach of UK law, please notify us by emailing [eprints@whiterose.ac.uk](mailto:eprints@whiterose.ac.uk) including the URL of the record and the reason for the withdrawal request.

1

## 2 **Main Manuscript for**

3 A multi-omics approach to lignocellulolytic enzyme discovery reveals a new ligninase  
4 activity from *Parascedosporium putredinis* NO1

5 Nicola C. Oates<sup>a</sup>, Amira Abood<sup>a</sup>, Alexandra M. Schirmacher<sup>a</sup>, Anna M. Alessi<sup>a</sup>, Susannah M. Bird<sup>a</sup>,  
6 Joseph P. Bennett<sup>a</sup>, Daniel R. Leadbeater<sup>a</sup>, Yi Li<sup>a</sup>, Adam A. Dowle<sup>b</sup>, Sarah Liu<sup>c</sup>, Vitaliy I. Tymokhin<sup>c</sup>,  
7 John Ralph<sup>c</sup>, Simon J. McQueen-Mason<sup>a</sup>, and Neil C. Bruce<sup>a</sup>

8

9 <sup>a</sup>Centre for Novel Agricultural Products, Department of Biology, University of York, York, YO10  
10 5DD, UK.

11 <sup>b</sup>Bioscience Technology Facility, Department of Biology, University of York, York, YO10 5DD, UK.

12 <sup>c</sup>Department of Biochemistry, and the Department of Energy's Great Lakes Bioenergy Research  
13 Center, Wisconsin Energy Institute, University of Wisconsin, Madison, WI, 53726, USA

14 Correspondence and requests for materials should be addressed to N.C.B.

15 **Email:** neil.bruce@york.ac.uk

## 16 **Classification**

17 Biological sciences: Applied Biological Sciences

## 18 **Keywords**

19 Lignocellulose, Lignin,  $\beta$ -etherase, Tricin, *Parascedosporium putredinis*

## 20 **Author Contributions**

21 N.C.B. and J.R. conceived the idea; N.C.O., S.J.M-M. and N.C.B. designed the experiments;  
22 N.C.O., A.A., A.M.S., A.M.A., S.M.B., J.P.B., D.L., Y.L., A.A.D. S.L and V.I.T. performed the  
23 research; N.C.O., A.A., A.S., J.P.B., D.R.L., Y.L., J.R., S.J.M-M. and N.C.B. analyzed data; N.C.O and  
24 N.C.B. wrote the manuscript with contributions from co-authors. All authors reviewed and  
25 approved the final manuscript.

26

27 **Abstract**

28 Lignocellulose, the structural component of plant cells, is a major agricultural byproduct and the  
29 most abundant terrestrial source of biopolymers on Earth. The complex and insoluble nature of  
30 lignocellulose limits its conversion into value-added commodities and, currently, efficient  
31 transformation requires expensive pretreatments and high loadings of enzymes. Here, we  
32 report on a fungus from the *Parascedosporium* genus, isolated from a wheat-straw composting  
33 community, that secretes a large and diverse array of carbohydrate-active enzymes (CAZymes)  
34 when grown on lignocellulosic substrates. We describe a new oxidase activity that cleaves the  
35 major  $\beta$ -ether units in lignin, thereby releasing the flavonoid triclin from monocot lignin, and  
36 enhancing the digestion of lignocellulose by polysaccharidase cocktails. We show that the  
37 enzyme, which holds potential for the biorefining industry, is widely distributed among  
38 lignocellulose-degrading fungi from the Sordariomycetes phylum.

39 **Significance Statement**

40 Lignocellulose, in the form of crop residues, presents an attractive alternative to crude oil for  
41 both the production of renewable fuels and chemicals. Its large-scale application as a feedstock,  
42 however, remains limited. A bottleneck in its implementation is the presence of lignin, a  
43 complex hydrophobic polymer, that envelopes the structure, physically blocking access to sugar-  
44 rich polymers that lie beneath. Here we describe the isolation of an exceptional lignocellulose-  
45 degrading fungus that produces a new oxidase activity with no cofactor requirements. This  
46 enzyme cleaves  $\beta$ -ether units in lignin releasing triclin, a flavonoid of pharmaceutical potential,  
47 from the lignin macromolecule. Furthermore, we demonstrate that treatments with this enzyme

48 can increase the digestibility of lignocellulosic biomass, offering the possibility of producing a  
49 valuable product from lignin while decreasing processing costs.

50

## 51 **Main Text**

52

## 53 **Introduction**

54

55 Photosynthetically-fixed carbon in lignocellulose is produced in vast quantities on the Earth's  
56 surface. The abundance of crop residue lignocellulose makes it an attractive alternative to crude  
57 oil in the production of renewable, low-carbon, fuels and chemicals (1). Effective utilization of  
58 lignocellulose, nevertheless, remains a challenge, as the extraction of sugars for fermentation  
59 requires intensive physicochemical pretreatments and high loadings of enzyme cocktails. A key  
60 factor in the recalcitrance of lignocellulose to degradation is lignin, a heterogeneous,  
61 hydrophobic aromatic polymer that encases the cellulose and hemicellulosic polysaccharides,  
62 blocking enzyme accessibility and impeding cellulase activity (2, 3).

63 Lignin is typically synthesized in secondary cell walls of higher plants through the phenoxy-  
64 radical coupling of the differentially methoxylated hydroxycinnamyl alcohols, sinapyl alcohol,  
65 coniferyl alcohol, and *p*-coumaryl alcohol, generating  $\beta$ -O-4, 4-O-5,  $\beta$ -5,  $\beta$ -1, 5-5 and  $\beta$ - $\beta$   
66 inter-unit linkages in  $\beta$ -ether, biphenyl ether, phenylcoumaran, spirodienone, biphenyl, and  
67 resinol units, respectively. Tricin [5,7-dihydroxy-2-(4-hydroxy-3,5-dimethoxyphenyl)-4*H*-  
68 chromen-4-one], an *O*-methylated flavone recognized for its pharmaceutical potential due to its  
69 antioxidant and antibacterial properties, with purported functions ranging from anti-tumor  
70 activity to potential diabetes suppression (4, 5). Tricin has been recently described to form part  
71 of the structure of lignin from monocotyledonous plants including wheat, rice, and sugarcane (6-  
72 9). To date, tricin has only been observed incorporated into the lignin structure via 4-O- $\beta$   
73 linkages, having arisen from the radical coupling of the flavone at its 4'-O-position with a

74 monolignol at its  $\beta$ -position. It is therefore reported to be a potential nucleation point at which  
75 lignification initiates in monocots, locating triclin at the (starting) terminus of the lignin  
76 macromolecule (8, 10). The selective extraction of triclin from monocots, which encompass the  
77 majority of agricultural biomass, using methods amenable to the lignocellulose biorefinery  
78 concept could potentially go some way towards mitigating the cost of second-generation biofuel  
79 production (11).

80 Despite extensive research into the biological degradation of lignocellulose and the mining  
81 of microbial communities for their ability to break down cellulose and hemicelluloses, questions  
82 persist over the biodegradation of lignin, and the mechanisms that facilitate its  
83 depolymerization. Although delignification involving manganese superoxidase dismutases (12),  
84 laccases, and dye-decolorizing peroxidases (13) by bacteria has been described, it is fungi that  
85 are the major lignin degraders in the terrestrial environment. Historically, wood-decaying fungi  
86 have been divided into white-, brown-, and soft-rots, depending on the morphology of their  
87 decomposition products. White-rot Basidiomycetous fungi, such as *Ceriporiopsis subvermispora*  
88 or *Phanerochaete chrysosporium*, are named for their ability to degrade and mineralize the  
89 dark-colored lignin and selectively enrich the white cellulose (14). This degradation is catalyzed  
90 through the action of oxidative enzymes (oxidoreductases) such as laccases, manganese  
91 peroxidases, dye-decolorizing peroxidases, and high-redox-potential heme-peroxidases (15, 16).

92 Conversely, although lignin modification has been recognized in brown-rot species (17, 18),  
93 significant solubilization does not occur. Instead, the degradative strategy is typified by the  
94 selective removal of the polysaccharide components from the plant cell wall through chemical  
95 and enzymatic means (19-21). Soft-rot fungi that, unlike the Basidiomycete white- and brown-  
96 rots, are usually Ascomycetes, deploy an alternative strategy. These fungi are capable of

97 extensively degrading lignocellulose through the secretion of large quantities of enzymes close  
98 to the site of attack due to the penetrating nature of their filamentous hyphae (22). This causes  
99 characteristic softening of the lignocellulose, as the plant cell walls lose their structural integrity.  
100 Ascomycetes are not, however, well known for their ability to solubilize lignin and, although  
101 there have been reports that they possess the capacity to modify and degrade lignin (23), it is  
102 not clear how this occurs.

103       Uncovering the mechanisms that govern lignin degradation by Ascomycetes, represents an  
104 opportunity to discover new enzyme systems that can be employed in biorefining applications.  
105 Here we report the discovery of an Ascomycete, *Parascedosporium putredinis* NO1, isolated  
106 from straw-enriched compost, that thrives in the latter stages of decomposition. We identify an  
107 extensive arsenal of lignocellulose-degrading enzymes during growth on wheat straw, and  
108 report on the abundance of secreted, and as yet, hypothetical proteins. In particular, we report  
109 the discovery of a new oxidase that can cleave the  $\beta$ -O-4 inter-unit structural linkage of lignin,  
110 releasing triclin from monocot biomass and boosting the digestion of the biomass by cellulases.  
111 Importantly, this enzyme does not require a cofactor.

112

## 113 **Results**

114

### 115 **Isolation of *Parascedosporium putredinis* NO1**

116 We inoculated liquid cultures containing wheat straw as the sole carbon source with homogenized  
117 samples of wheat straw-enriched compost. From these we tracked the dynamics of the resulting  
118 microbial community. Sequencing of 16S ribosomal RNA genes generated over three million reads  
119 from the prokaryotic community over the whole timecourse, which clustered together to form  
120 25,304 operational taxonomic units (OTUs) (Fig. 1A). The most abundant bacterial phyla identified

121 were the gram-negative *Bacteroidetes*, *Verrucomicrobia* and *Proteobacteria*, respectively,  
122 representing an average of 31, 19.8 and 15.5% of the total reads across the time course. Analysis  
123 of the eukaryotic community by sequencing the Internal Transcribed Spacer (ITS) region  
124 predominantly yielded reads that had no match within the UNITE fungal rDNA sequence database  
125 (24, 25). In total, 96.5% of generated OTUs were not recognized as fungal and instead showed the  
126 closest homologies to protozoa. Among the fungi, we noted distinct changes in the composition  
127 of the community with time. In particular, a fungus (designated strain NO1) an Ascomycete in the  
128 Microascaceae family, showed increased abundance after 4 weeks of incubation (Fig. 1B). Reads  
129 assigned to genus *Graphium* dominated the eukaryotic community in the shake flasks after four  
130 weeks of incubation, representing 84% of the identifiable fungal reads at 8 weeks, a time point by  
131 which, we hypothesize, the majority of easily accessible carbon from wheat straw has been  
132 depleted (26). A synamorph of *Graphium*, *Parascedosporium putredinis* strain NO1 identified  
133 through ITS and 18S analysis was readily isolated from shake flasks by culturing on both nutrient  
134 agar and potato dextrose agar. Interestingly, this fungus could be selectively cultivated when agar  
135 plates contained kraft lignin as the sole carbon source.

#### 136 **Omics analysis of wheat straw degradation by *P. putredinis* NO1**

137 We confirmed that *P. putredinis* NO1 could grow on wheat straw as a sole carbon source and  
138 optimized the composition of growth media for cellulase and xylanase production (*SI Appendix*,  
139 Fig. S1). The deconstruction of wheat straw by *P. putredinis* NO1 over 28 days was tracked by  
140 measuring mass loss and carbohydrate-active enzyme (CAZy) activity (*SI Appendix*, Fig. S2). This  
141 growth experiment identified the second, fourth and tenth day of incubation on wheat straw as  
142 distinct time points to harvest RNA for sequence analysis, chosen because together they  
143 represent the first detection of lignocellulolytic activity (day 2), the peak of enzyme activities (day

144 4) and the subsequent reduction of lignocellulolytic activity (day 10) – a point at which the easily  
145 accessible sugars in the wheat straw had been utilized. RNA was also harvested from *P. putredinis*  
146 grown on glucose for four days.

147 After sequencing, 5,586 unique contiguous DNA sequences (contigs) were assembled from  
148 339,854,704 reads, and differential gene analysis identified 2,189 contigs that were upregulated  
149 at high confidence and fold-change ( $P < 0.001$ ,  $FC > 10$ ) between growth on wheat straw compared  
150 to glucose. These highly upregulated genes included those coding for 102 putative CAZy proteins;  
151 47 glycoside hydrolases (GH), 41 auxiliary activities (AA), ten carbohydrate esterases (CE) and a  
152 polysaccharide lyase (PL), the majority of which were upregulated after four days of growth (Fig.  
153 2), in agreement with the peak of the observed enzymatic activities in *P. putredinis* NO1 culture  
154 supernatants.

155 As the macromolecular structure of lignocellulose prohibits intracellular degradation,  
156 enzymes for its deconstruction are typically secreted. To capture these enzymes, we performed  
157 LC-MS/MS analysis on protein samples collected directly from the culture supernatant, and  
158 separately, from those bound to insoluble components of the culture using a biotin-labelling  
159 method (27). From across all samples, 3,671 proteins were identified, including 1,037 proteins  
160 present in only wheat straw conditions (*SI Appendix*, Fig. S3A) and 275 sequences that contained  
161 a recognizable CAZy domain (*SI Appendix*, Dataset S1). These putative carbohydrate-  
162 deconstructing enzymes accounted for 25.2% (192 proteins) of the molar percentage of the  
163 supernatant samples and 13.9% (171) of the biotin-labelled samples after four days of growth  
164 on wheat straw, compared to 13.3% (97) of the supernatant and 2% (56) of the biotin labelled  
165 samples from glucose-grown cultures (*SI Appendix*, Fig. S3B).



166 The most abundant CAZy family, 3.7% and 3.6% of the respective supernatant and biotin-  
167 labelled fractions on the fourth day, were GH6s (Fig. 3). These, along with GH7s, often constitute  
168 the major cellulases in filamentous fungi (28), and may be endoglucanases or processive  
169 cellobiohydrolases. Other GH families that are likely active on cellulose, including the GH7  
170 (typically cellobiohydrolases or endoglucanases), GH5 and GH45 (often endoglucanases), and  
171 GH1 and GH3 (typically glucosidases) families (29), were also prominent within the secretome.

172 Efficient lignocellulose deconstruction, however, demands a combination of cellulolytic and  
173 hemicellulolytic enzymes that work cooperatively. Enzymes related to the depolymerization of  
174 arabinoxylan (the major hemicellulose in wheat straw), were well represented within the  
175 exoproteome. Nine proteins were identified with homology to endo  $\beta$ -1,4-xylanases (GH10 and  
176 GH11) that hydrolyze the arabinoxylan backbone, and five proteins were identified as putative  
177  $\beta$ -1,4-xylosidases that act on the resultant fragments to produce xylose monomers (GH3, GH31,  
178 GH43\_1, GH43\_11, GH43\_36). Also of note, were the GH43 subfamilies GH43\_1, GH43\_21,  
179 GH43\_22, GH43\_26 and GH43\_36 that were abundant within the secretome, and include  
180 putative  $\beta$ -D-xylosidases,  $\alpha$ -L-arabinofuranosidase, and  $\beta$ -1,3-galactosidase activities.

181 Three proteins, belonging to the CE1 family, showed significant sequence homology to  
182 feruloyl esterases. Ferulate acylates the arabinose side-chain of arabinoxylans, and through the  
183 formation of diferulate bridges and ester-ether linkages allows the respective formation of  
184 covalent interactions between arabinoxylan chains (with each other) and with lignin. Feruloyl  
185 esterases, therefore, are thought to aid the solubilization of plant cell wall polysaccharides by  
186 the hydrolysis of the ester link that exists between ferulic acid residues and arabinose, thereby  
187 disrupting the cross-linking of cell wall components (30). Putative acetyl xylan esterases (3 in  
188 CAZy family CE1 and 3 in CE5) were also observed and are known to facilitate the degradation of

189 xylan through the removal of acetyl substitutions that render the substrates more recognizable  
190 by polysaccharidase enzymes (31).

191 The CAZy auxiliary activity (AA) class is classified as containing enzymes that act in conjunction  
192 with carbohydrate-active enzymes through redox activities. Interestingly, 69 putative proteins  
193 from the AA class were detected in the exosecretome, more than many lignocellulose-degrading  
194 fungi contain in their total genome (32), suggesting an important role for the oxidative  
195 degradation of lignocellulose in *P. putredinis* NO1. The AA9 family were highly represented  
196 within the exosecretome. This family, along with the AA10, AA11, AA13, AA14 and AA15  
197 families, constitutes the lytic polysaccharide monooxygenases (LPMOs) – a class of copper  
198 metalloenzymes that catalyze the oxidative cleavage of glycosidic bonds in multiple  
199 polysaccharide substrates including chitin, cellulose, and xylan (33, 34). In total, we identified  
200 nineteen putative LPMOs (16 AA9s; 2 AA11s; 1 AA13), fifteen of which were upregulated tenfold  
201 or more between glucose and wheat straw conditions. Fittingly, 16 AA3s (glucose-methanol-  
202 choline (GMC) oxidoreductase) and 9 AA7s (glucosylglycerol oxidase), which have been  
203 shown to facilitate the activity of the LPMOs through electron shuttling (35, 36), were also  
204 present within wheat straw cultures.

205       Established lignin depolymerizing enzymes associated with the white-rot fungal decay of  
206 lignin, including laccases from the AA1\_1 subfamily (37, 38), or peroxidases from the AA2 family  
207 (14), were not present within the libraries. This is perhaps not surprising given that *P. putredinis*  
208 NO1 sits within the Ascomycota phylum, and as such is closer in relation to the soft-rots.

209       Five putative multicopper oxidase proteins were also observed – two from the AA1\_3  
210 subfamily (Laccase-like multicopper oxidase) and one from the AA1\_2 subfamily (Ferroxidase).  
211 Laccase-like multicopper oxidases are of unknown function but have been implicated in lignin

212 degradation, as well as other diverse functions (iron homeostasis, offense/defense) (39),  
213 whereas ferroxidases have been reported to be involved in lignocellulose degradation in  
214 Ascomycetes, in which they generate hydroxyl radicals via the Fenton reaction (40).

215 Despite the apparent lack of known ligninases in *P. putredinis* NO1, a putative AA6 (1,4-  
216 benzoquinone reductase) associated with the intracellular biodegradation of aromatic  
217 compounds was present within the supernatant and may have a role in the metabolism of lignin  
218 breakdown products (32, 41).

219 Of key interest to us was the potential of *P. putredinis* NO1 to produce novel lignocellulolytic  
220 activities, particularly those able to boost lignocellulose deconstruction via the modification and  
221 solubilization of lignin. An unknown protein, c2092\_g1\_i1, identified in the exosecretome was  
222 subsequently found to have  $\beta$ -etherase activity and no CAZy identification.

### 223 **A new oxidase displaying $\beta$ -etherase activity**

224 The  $\beta$ -ether motif, with its characteristic  $\beta$ -O-4 inter-unit linkage, is the most abundant in lignin,  
225 estimated at representing over 50% of the total inter-unit linkages (42). Enzymes employing  $\beta$ -  
226 ether cleavage mechanisms can deconstruct synthetic and extracted lignin (43-45); these  
227 bacterial etherases that have been characterized to date, however, are intracellular proteins,  
228 and are glutathione- or NAD<sup>+</sup>- dependent, suggesting that in nature they are not directly  
229 involved in the breakdown of the lignin macromolecule, but rather its smaller, membrane-  
230 transportable oligomers. An extracellular fungal protein displaying  $\beta$ -etherase activity was  
231 previously purified from the supernatant of the *Chaetomium* sp. 2BW- 1, although its identity  
232 remains unknown (46).

233 Using a synthetic lignin model compound, GG $\beta$ 4MU (7-[2-hydroxy-2-(4-hydroxy-3-  
234 methoxyphenyl)-1-(hydroxymethyl)ethoxy]-4-methyl-2H-1-benzopyran-2-one), containing a  $\beta$ -

235 methylumbelliferyl ether, guaiacylglycerol- $\beta$ -(4-methylumbelliferyl) ether that when cleaved  
236 yields the fluorogenic product 4-methylumbelliferone (4MU) (*SI Appendix*, Fig. S4) (47), we  
237 detected  $\beta$ -etherase activity within the culture supernatant of *P. putredinis* NO1. This activity  
238 was present when *P. putredinis* NO1 was grown on wheat straw but not on glucose, suggesting a  
239 possible role in lignocellulose degradation, and appeared to be independent of cofactors such as  
240 glutathione or NAD<sup>+</sup>. Given its presence in the secretome and its apparent cofactor  
241 independence, we hypothesized that this putative ligninase was unlikely to share significant  
242 sequence homology to the previously described intracellular  $\beta$ -etherases from sphingomonads,  
243 and indeed no proteins with similarity to these enzymes were detected. We, therefore,  
244 subjected the culture supernatant of *P. putredinis* NO1 grown on wheat straw to a series of  
245 protein fractionation techniques, enriching at each step for  $\beta$ -etherases activity.

246 The putative  $\beta$ -etherase was initially purified by ammonium sulfate precipitation of the  
247 proteins in the culture supernatant to decrease sample pigmentation and reduce protein-  
248 protein interactions. This treatment facilitated further purification by size-exclusion and anion-  
249 exchange chromatography. Using shotgun proteomics, we identified c2092\_g1\_i1, a 44.5 kDa  
250 protein present in the purified fraction that contained a predicted signal peptide. Analysis of the  
251 transcriptomic and proteomic data revealed this protein was strongly upregulated in the  
252 presence of wheat straw and present in both the supernatant and biotin-labelled proteomic  
253 libraries throughout the growth of *P. putredinis* NO1 on wheat straw (*SI Appendix*, Fig. S5). Using  
254 profile Hidden Markov models constructed by HMMER3 on using the pFAM database (48), we  
255 saw homology to a common central tyrosinase domain (PF00264; Evalue = 7.1e-49) with a  
256 characteristic binuclear type-3 copper-binding site consisting of six histidine residues located in  
257 a four-helical bundle coordinating the binding of two copper ions (49) (*SI Appendix*, Fig. S6).

258 Mushroom tyrosinase (*Agaricus bisporus*), has been reported to have promiscuous  $\beta$ -etherase  
259 activity on small synthetic compounds but no significant activity has been reported against  
260 macromolecular lignin (50). Fungal tyrosinases (polyphenol oxidases) are predominantly  
261 associated with pigmentation and browning; specifically, through melanin production, whereby  
262 they catalyze the introduction of a hydroxyl group *ortho* to the phenol in a *para*-substituted  
263 monophenol and the subsequent oxidation to the corresponding *o*-quinone (51). However,  
264 c2092\_g1\_i1 lacks both the C- and N-terminal domains that tyrosinases typically contain and  
265 instead shows higher homology (170/370 identity (46%)) to a catechol oxidase (AoCO4) from  
266 *Aspergillus oryzae* (52), which differs from tyrosinases due to a lack of mono-oxygenase activity  
267 (53). Examination of the proteomics library resulted in the identification of seven sequences  
268 with significant similarities to c2092\_g1\_i1 (*SI Appendix*, Table S1), all predicted to be  
269 extracellular and soluble, and five upregulated in the presence of wheat straw (*SI Appendix*, Fig.  
270 S7). Searches within the NCBI non-redundant database further revealed the presence of  
271 proteins of similar sequence (>50% sequence identity) distributed throughout fungal genomes  
272 of the Sordariomycetes class of Ascomycetes (*SI Appendix*, Table S2, Fig. S8).

### 273 **Experimental confirmation of $\beta$ -etherase activity**

274 To determine if c2092\_g1\_i1 was responsible for the observed  $\beta$ -etherase activity, we  
275 heterologously expressed the codon-optimized sequence in *Escherichia coli*. The recombinant  
276 protein was purified (*SI Appendix*, Fig. S9), and the  $\beta$ -etherase activity of the protein was  
277 confirmed by determining the level of fluorescence released after incubation with GG $\beta$ 4MU (*SI*  
278 *Appendix*, Fig. S10A). In reaction conditions absent of oxygen, we confirmed the oxidative  
279 nature of this protein, seeing a near total reduction in activity when the assay was conducted  
280 under anaerobic conditions (*SI Appendix*, Fig. S10B).

281 The pH and temperature dependency of the enzyme were investigated, revealing maximum  
282 activity at pH 10 and 60 °C (*SI Appendix*, Fig. S10C and D). The *P. putredinis* NO1 oxidase did not  
283 display activity against L-tyrosine and L-DOPA, as is characteristic for tyrosinases (*SI Appendix*,  
284 Fig. S11) (54). We subsequently assayed for potential oxidase activity against a range of phenolic  
285 substrates, including di-phenolics, known to be catechol oxidase substrates (53), and observed  
286 no similarities to catechol oxidase in terms of substrate preference (*SI Appendix*, Fig. S12, Table  
287 S4). Interestingly, activity was seen with the substrates: 4-hydroxybenzoic acid, vanillic acid, and  
288 quercetin, all known to be tyrosinase inhibitors (55).

#### 289 **Release of triclin and lignin units from wheat straw**

290 Tricin has recently been described as a subunit in the lignin of monocot species, incorporated  
291 through a 4-O- $\beta$  linkage (11). As wheat straw contains relatively high concentrations of triclin  
292 compared to other agriculturally relevant feedstocks (8), we assessed the ability of the oxidase  
293 to release triclin from wheat straw. The oxidase was incubated with wheat straw for sixteen  
294 hours under physiological conditions (pH 8.5 and 30 °C). Reaction products were monitored by  
295 High-Performance Liquid-Chromatography (HPLC), and a peak corresponding to triclin was  
296 identified by reference to an authentic standard and confirmed by mass spectrometry. Under  
297 the growth conditions used for *P. putredinis* NO1, a significantly higher concentration of triclin  
298 was present in the reaction supernatant of wheat straw with the purified protein fractions  
299 compared to incubations with buffer alone (ANOVA,  $F(2,12)=44.67$ ,  $p<0.05$ ) (Fig. 4A). We were  
300 also able to detect the presence of *p*-coumaric acid, vanillin, and *p*-hydroxybenzaldehyde in the  
301 reaction supernatant through comparisons with authentic standards and mass spectrometry;  
302 however, unlike triclin, these compounds were not enriched under the enzyme-treated reaction

303 conditions (*SI Appendix*, Fig. S13) and presumably are produced as a result of simple ester  
304 cleavage.

305 NMR (Fig. 5) of the enzyme lignins (EL) isolated (following crude polysaccharidase treatment  
306 to saccharify most of the polysaccharides) (56), and the product generated from it by a non-  
307 optimized treatment with our enzyme showed little change to the actual lignin profile but a  
308 strong decrease in the triclin level. Thus, even though integration of correlation contours in the  
309 spectra resulting from such 2D-HSQC (heteronuclear single-quantum coherence) experiments  
310 does not provide reliable quantification, their relative values are considered to be valid (57, 58).  
311 Analysis showed that the relative triclin ether level in the lignin dropped from nearly 12% in the  
312 control to about 8.5% after the treatment. We were initially disappointed that we couldn't  
313 detect similar reductions in levels of the  $\beta$ -ether units **A** (Fig. 5), but caution that these are  
314 'quantified' on an A+B+C=100% basis and it is easy to speculate on how the levels might not  
315 significantly change even with some (presumably low-level)  $\beta$ -ether cleavage; in changing the  
316 basis to a level per 100 aromatic (S+G+H) units as previously used (7, 23), the values (Fig. 5) do  
317 confirm a modest drop (67 down to 65) in  $\beta$ -ether units **A** specifically. In spectra from the whole  
318 cell wall component (and not just the isolated lignin, not shown), the trends were similar and  
319 the T<sub>6</sub> and T<sub>8</sub> contours were particularly weak in the treated sample whereas the T<sub>2</sub>'/6' peak  
320 was relatively strong; we have noted this occurrence before in rapidly relaxing samples, and do  
321 not fully understand its origin; regardless, the relative triclin level in the treated material was  
322 again lower than in the control and obviously consistent with the measured release of triclin  
323 noted above.

324 As mushroom tyrosinase has been reported to cleave  $\beta$ -ether linkages promiscuously (50),  
325 we tested its  $\beta$ -etherase activity on wheat straw under equivalent conditions. We observed less

326 tricin production in the reaction mixtures containing mushroom tyrosinase compared to the *P.*  
327 *putredinis* NO1 enzyme treatments. As tricin is a known tyrosinase inhibitor that binds non-  
328 competitively to the hydrophobic pocket of the protein (59), and *p*-coumaric acid has been  
329 characterized as having a mixed-type inhibition effect (60), inhibition through the non-reversible  
330 binding of the reaction products, could go some way to explaining why mushroom tyrosinase  
331 displays little activity towards the lignin macromolecule.

### 332 **Enzyme pretreatment boosts saccharification**

333 To investigate if a pretreatment of wheat straw with the *P. putredinis* NO1 oxidase would  
334 improve saccharification rates, we incubated wheat straw with enzyme for sixteen hours before  
335 the addition of commercial cellulases, and observed a 20% increase in the level of glucose  
336 released compared to wheat straw treated with buffer alone (ANOVA,  $F(2,12)=4.47$ ,  $p<0.05$ )  
337 (Fig. 4B).

338

### 339 **Discussion**

340 *P. putredinis* NO1 is able to dominate cultures in the latter stages of wheat straw degradation in  
341 a mixed microbial community when easily accessible polysaccharides have been exhausted.  
342 Using a combination of 'omics approaches, we have identified a diverse range of potentially  
343 industrially relevant carbohydrate-active enzymes, including a large number of enzymes  
344 associated with the oxidative attack on lignocellulose. In particular, we have identified a new  
345 extracellular oxidase that is preferentially expressed in the presence of wheat straw and  
346 demonstrated that this enzyme can release the pharmaceutically relevant flavonoid tricin from  
347 monocot lignin. We also demonstrated that pre-treatment with the oxidase can significantly  
348 boost the saccharification of wheat straw when used with a commercial cellulase cocktail.



349 Whether this is a direct effect of increased carbohydrate availability due to lignin removal or a  
350 boosting effect of the oxidase on components of the saccharification cocktail remains to be  
351 established. We contend that this ability to deconstruct and modify lignin is important for *P.*  
352 *putredinis* NO1 to be able to out-compete other microbial species during the latter stage of  
353 plant biomass degradation when easily accessible lignocellulose components are depleted.  
354 In a recent report, the ascomycete fungus *Podospora anserina* was observed to possess  
355 ligninolytic activities, and analysis of the residual lignin after fungal growth on wheat straw  
356 demonstrated a decrease in triclin. *P. anserina* encodes for a number of proteins which share  
357 homology to the enzyme described here, two of which were detected in the proteome of *P.*  
358 *anserina* when cultured with wheat straw lignin (23). Preferential removal of triclin subunits has  
359 also been described by the white-rot fungi, *Pleurotus eryngii*, during the selective delignification  
360 of wheat straw and has been proposed to be key to lignocellulose degradation, although the  
361 enzyme activity that facilitated triclin release was not identified (61). When the publicly available  
362 genome of *P. eryngii* was examined for the presence of proteins with homology to the oxidase  
363 from *P. putredinis* NO1, no significant hits were detected.

364 As the protein described as being responsible for  $\beta$ -etherase activity from *Chaetomium* sp.  
365 2BW-1 was not identified to sequence level, it is unclear whether it shares homology to the  
366 enzyme described here; however, the proteins appear to be distinct as the reported sizes differ  
367 by 20 kDa (46). Taken together, these observations suggest that multiple, structurally dissimilar,  
368 enzymes in the natural environment may mediate ether linkage disruption in lignocellulose-  
369 degrading microbes.

370 This enzymes ability to release triclin from lignin and could have potential biotechnological  
371 applications. To the best of our knowledge, this is the first identification and characterization of

372 an extracellular enzyme capable of  $\beta$ -ether cleavage that has no cofactor requirement for  
373 activity.

374

## 375 **Materials and Methods**

376

### 377 **Methods**

#### 378 **Wheat straw degradation in shake-flasks inoculated with compost**

379 Wheat straw compost that had developed over a year, was used to inoculate 1 L minimal media  
380 cultures that had been supplemented with 5% (w/v) milled wheat straw. Flasks were incubated  
381 at 30 °C and shaken at 150 rpm. The minimal media contained KCl 0.52 g/L, KH<sub>2</sub>PO<sub>4</sub> 0.815 g/L,  
382 K<sub>2</sub>HPO<sub>4</sub> 1.045 g/L, MgSO<sub>4</sub> 1.35 g/L, NaNO<sub>3</sub> 1.75 g/L, and Hutner's trace elements and was based  
383 on *Aspergillus niger* minimal media (62). Spread plates on nutrient agar (NA) and potato  
384 dextrose agar (PDA) were created weekly from serial dilutions.

#### 385 **Targeted amplicon sequencing of 16S and ITS region**

386 Genomic DNA was harvested from the compost cultures using a modified CTAB protocol as  
387 described by Alessi *et al.* (26). Phusion® High-Fidelity DNA Polymerase (Finnzymes OY, Finland)  
388 was used to generate amplicons for sequencing. These were purified using Agencourt AMPure  
389 XP (Beckman Coulter). Sequencing was performed using an Ion Torrent platform at the  
390 Biorenewable Development Centre, York, U.K. The primer pairs, were as follows; ITS1 Fw –  
391 TCCGTAGGTGAACCTGCGG, Rv – CGCTGCGTTCATCG (63), 16S Fw – AYTGGGYDTAAAGNG, Rv  
392 – TACNVGGGTATCTAATCC (64), for ITS and 16S sequencing respectively. Resultant sequences  
393 were demultiplexed, primer sequences were removed and reads adjusted for orientation. Reads  
394 without recognizable primer sequences and under 180 bp were filtered out. Remaining reads  
395 were then analyzed using Qiime (65). The open- reference operational taxonomic unit (OTU)  
396 picking process was used, before taxonomy was assigned using the greengenes gg\_13\_8 97 otus  
397 database (66, 67) and the UNITE (alpha release 12\_11) database (68) for bacterial and fungal  
398 identification respectively.

399

#### 400 **Central composite design for media optimization**

401 A central composite design with rotation (69) was used to optimize media for the production of  
402 cellulase and xylanase activity after seven days of incubation in minimal media with 1.5 % wheat  
403 straw, as described in Oates (70). Cellulase and xylanase activity was assessed by incubating  
404 supernatant on carboxymethylcellulose (CMC) or xylan (beechwood) and measuring reducing  
405 sugar release. The sodium nitrate concentration was varied between 0 g/L and 3.5 g/L, and yeast  
406 extract was varied between 0% and 1% (w/v). The optimized media for *P. putredinis* NO1 growth  
407 consisted of yeast extract 8.55 g/L, KCl 0.52 g/L, KH<sub>2</sub>PO<sub>4</sub> 0.815 g/L, K<sub>2</sub>HPO<sub>4</sub> 1.045 g/L, MgSO<sub>4</sub> 1.35  
408 g/L, NaNO<sub>3</sub> 1.75 g/L and Hutner's trace elements.

409

#### 410 **Characterization of *P. putredinis* NO1 growth on wheat straw**

411 Biomass, that had been gently rinsed with x1 PBS, was flash-frozen in liquid nitrogen and  
412 lyophilized to calculate the dried weight of cultures. To estimate total protein, aliquots of 100 µg  
413 of this biomass was boiled in 0.2 % (w/v) sodium dodecyl sulfate (SDS) for 5 mins, and vigorously  
414 vortexed, before supernatant was collected through centrifugation. This was repeated three  
415 times. Five-volumes of ice-cold acetone was used to precipitate protein overnight at -20 °C and  
416 protein pellets were collected via centrifugation, washed with 80 % v/v ice-cold ethanol and  
417 resuspended in H<sub>2</sub>O, before being quantified using the Bradford assay.

418 To measure the amount of reducing ends produced after incubation of supernatant on  
419 polysaccharides, 10 µL of cultural supernatant was incubated with 2% (w/v) of either CMC or  
420 xylan (beechwood) in 200 µL of 50 mM sodium phosphate at 6.8 at 30 °C, before the Lever assay  
421 (71) was used to calculate reducing ends at set timepoints. Standard curves were generated  
422 using either glucose or xylose.

#### 423 **RNA extraction from *P. putredinis* NO1**

424 RNA was extracted from cultures of *P. putredinis* NO1 that had been incubated at 30 °C with  
425 shaking at 180 rpm (70). Optimized growth media was used, supplemented with either 1.5 %  
426 wheat straw or 0.5 % glucose. At set time points, aliquots of either 0.5 g, 0.3 g or 0.1 g were  
427 taken, and 1 mL of Trizol (Life Technologies) and 3x3 mm tungsten carbide beads were added to  
428 disrupt cells in a TissueLyser II (Qiagen) for 2x2 min. Once the cells were disrupted the standard  
429 Trizol method was used to purify RNA as per manufacturer's instruction. DNA contamination

430 was removed with RTS DNase kits (Mobio) followed by treatment with ZymoResearch RNA Clean  
431 & Concentrator™ 5 kits. Ribo-Zero™ Magnetic Epidemiology rRNA removal kits  
432 (RZE1224/MRZ11124C; Illumina) were used to enrich for mRNA.  
433 Sequencing was performed at The Genome Analysis Centre (TGAC), Norwich, U.K. Using the  
434 TruSeq RNA v2 protocol (Illumina 15026495 Rev.B). cDNA libraries were created before being  
435 normalized, pooled and diluted to a final concentration of 10 pM with 1% PhiX. Hybridization  
436 and first extension was performed using the TruSeq Rapid PE Cluster Kit v1 on the Illumina  
437 cBotTemplate, then transferred onto the Illumina HiSeq2500 for the remaining 100 cycles.  
438 Reads were trimmed to remove adaptor sequences with the ngsShoRT\_2.1 method, and pooled  
439 libraries were assembled by Trinity Software and used as reference in subsequent analysis. The  
440 raw data was subject to rRNA removal by catching the remaining paired reads after mapping to  
441 a modified rRNA\_115\_tax\_silva\_v1.0 ribosomal set, using BOWTIE2. The original reads of the  
442 individual libraries were mapped to the reference using BWA software package with default  
443 parameters and the number of reads counted using SAMtools software package for each contig.  
444 Putative open readings frames (ORFs) were selected by translating regions over 300 bp between  
445 potential start and stop codons. BLASTp was used to perform searches against the non-  
446 redundant protein database, HMMER3 was used to search the Pfam and dbCAN databases (48,  
447 72, 73), BLAST+ 2.3.0 (74) was used to perform local BLAST searches and SignalP 4.0 (75) was  
448 used to predict the presence of signal peptides.

#### 449 **Proteomic LC-MS/MS**

450 Supernatant proteins were collected from the culture supernatant in 20 mL aliquots. These were  
451 precipitated overnight in five volumes of ice-cold acetone, pelleted through centrifugation at  
452 10,000 xg, washed with 80 % ice-cold acetone and resuspended in 0.5 x PBS with 0.1% SDS. Two-  
453 gram samples of biomass were used to extract biomass-bound proteins, as described in Alessi *et*  
454 *al* (27). Both supernatant and biomass bound proteins were loaded into 4-12% (w/v) Bis-Tris  
455 acrylamide gels, separated with electrophoresis for 20 min and stained with InstantBlue (Sigma-  
456 Aldrich). Gel slices were analyzed as described previously (70). They were washed with 50% (v/v)  
457 aqueous acetonitrile containing 25 mM ammonium bicarbonate, reduced with 10 mM DTE and  
458 S-carbamidomethylated with 50 mM iodoacetamide and dehydrated with acetonitrile. Digests  
459 were performed overnight with 0.2 µg trypsin (Promega) at 37 °C in 25 mM ammonium

460 bicarbonate. After extraction with 50% (v/v) aqueous acetonitrile, peptides were vacuum dried  
461 and resuspended in 0.1% (v/v) aqueous trifluoroacetic acid. These were loaded onto a  
462 nanoAcquity UPLC system (Waters) with a nanoAcquity Symmetry C18, 5  $\mu\text{m}$  trap (180  $\mu\text{m}$  x 20  
463 mm Waters) and a nanoAcquity HSS T3 1.8  $\mu\text{m}$  C18 capillary column (75 mm x 250 mm, Waters).  
464 After washing the trap with 0.1% (v/v) aqueous formic acid (solvent A), a gradient solvent A and  
465 acetonitrile containing 0.1% (v/v) formic acid (solvent B) was used to separate peptides. The  
466 gradient proceeded from 2% to 30% of solvent B over 125 minutes linearly, then up to 50% over  
467 five min, before rising to 95% solvent B for 2.5 min. Between each injection, the column was  
468 equilibrated to the initial conditions for 25 min. The column temperature was 60 °C and the flow  
469 rate was 300 nL min<sup>-1</sup>. AutoMSMS mode was used to acquire positive ESI- MS & MS/MS spectra.  
470 Compass 1.7 software (microTOF control, Hystar and DataAnalysis, Bruker Daltonics) was used  
471 for instrument control with the following settings: ion spray voltage: 1,450 V; dry gas: 3 L min<sup>-1</sup>;  
472 dry gas temperature 150 °C; collision RF: 1,400 Vpp; transfer time: 120 ms; ion acquisition  
473 range: m/z 150-2,000. An absolute threshold of 200 counts and preferred charged state of 2-4  
474 was specified. Singly charged ions were excluded. Cycle time: 1 s, MS spectra rate: 5 Hz, MS/MS  
475 spectra rate: 5 Hz at 2,500 cts increasing to 20 Hz at 250,000 cts or above. Using the AutoMSMS  
476 fragmentation table, collision energy and isolation width settings were automatically calculated.  
477 For each precursor, a single MS/MS spectrum was acquired, and unless the precursor intensity  
478 increased fourfold a dynamic exclusion for 0.8 min was applied.  
479 The ORF library from *P. putredinis* NO1 was used as a reference to match the resultant spectra  
480 against, using Mascot (Matrix Science Ltd., version 2.4) run through the Bruker ProteinScape  
481 interface (version 2.1). Carbamidomethyl (C) and oxidation (M) were considered as fixed and  
482 variable modifications, respectively. MS/MS tolerance was 0.1 Da and peptide tolerance was 10  
483 ppm. A decoy database was used to attain a global false discovery rate of 1% using 'Mascot  
484 Percolator' and peptides were adjusted to only be accepted with a expect score of 0.05 or  
485 lower. Exponentially modified Protein Abundance Index (emPAI) was calculated as described by  
486 Ishihama (76), which could be normalized to give molar percentage values by dividing against  
487 the sum of all emPAI values for each sample. The R package BioStrings (77) was used to retrieve  
488 each protein sequence from the ORF library.  
489

490 **Synthesis of synthetic substrate GG $\beta$ 4MU (7-[2-hydroxy-2-(4-hydroxy-3-methoxyphenyl)-1-**  
491 **(hydroxymethyl)ethoxy]-4-methyl-2H-1-benzopyran-2-one).**

492 The synthetic substrate GG $\beta$ 4MU was synthesized in 6 steps according to the protocol reported  
493 by Weinstein and Gold starting from acetovanillone (47). The pure substrate GG $\beta$ 4MU was  
494 obtained as a white solid following purification using plate chromatography on silica-gel (10%  
495 v/v MeOH in CH<sub>2</sub>Cl<sub>2</sub>). The NMR data were in excellent agreement with those previously  
496 reported.

497 **Identification of  $\beta$ -etherase from native supernatant**

498 *P. putredinis* NO1 was cultivated in medium containing 1.5% wheat straw. The supernatant was  
499 filtered through mirapore cloth and the protein of interest purified. Briefly, filtered culture  
500 supernatant with 0.1% Tween20 was concentrated in a 50 mL stirred Ultracentrifugation Cell  
501 (Millipore Corporation, USA) with a Biomax 30 kDa Ultrafiltration Membrane (Millipore  
502 Corporation, USA). Ammonium sulfate was slowly added to the filtered culture supernatant to a  
503 concentration of 20% while stirring at 4 °C. The solution was centrifuged at 10,000 g for 15 min.  
504 The pellet was then resuspended in 2 mL buffer A (50 mM Tris-HCl, 100 mM NaCl, 0.1% Tween  
505 20, pH 8.5). Additional cuts were performed with 30, 40 and 50% ammonium sulfate. After  
506 assessing the fractions with the GG $\beta$ 4MU assay, samples were purified on a Superdex-200 (GE  
507 Healthcare, US), using the ÄKTA system and 50 mM Tris-HCl, 100 mM NaCl, 0.1% Tween 20, pH  
508 8.5. The most active sample was further purified using anion exchange chromatography. Anion-  
509 exchange chromatography was conducted on a DEAE FF column (GE Healthcare, US) with an  
510 increasing salt concentration from 0 to 1 M NaCl in 20 min (5 mL/min). A running buffer of 30  
511 mM Tris-HCl, 0.1% Tween 20, at various pH (7.0/7.4/8.5) was used. The Elution buffer was 30  
512 mM Tris-HCl, 1 M NaCl, 0.1% Tween 20.

513 **Production of recombinant  $\beta$ -etherase**

514 The c2092\_g1\_i1 gene was codon-optimized for expression in *E. coli* and synthesized into  
515 pET151 vector with N-terminal His-tag by Invitrogen. The expression plasmid was transformed  
516 into Arctic Express (DE3) competent cells. Auto-induction media was used for protein  
517 production. Inoculated cultures were incubated at 30 °C with shaking at 180 rpm until an optical  
518 density of 0.6 at 600 nm was reached. The temperature was then reduced to 11 °C for 48 h

519 before cell pellets were collected by centrifugation at 7000 rpm and 4 °C for 15 min.  
520 Supernatant was discarded, and pellets were suspended in 5 mL per 100 mL of starting culture  
521 20 mM (4-(2-hydroxyethyl)-1-piperazineethanesulfonic acid) (HEPES) pH 8, before sonicated on  
522 ice using a Misonix S-4000 sonicator at 70 kHz for 4 min, and a standard program of 3 s off  
523 followed by 7 s on. The pellet was collected after centrifugation and washed with 20 mM HEPES,  
524 2 M Urea, 0.5 M NaCl, 2% Triton™ X-100, pH 8, using the same volume as before, sonicated  
525 and pelleted. The resultant pellet was then resuspended in 20 mM HEPES, 0.5 M NaCl, 5 mM  
526 imidazole, 6 M guanidine hydrochloride, 1 mM dithiothreitol (DTT) pH 8, using 10 mL per 100 mL  
527 of original cell culture, to solubilize inclusion bodies. After pelleting through centrifugation for a  
528 final time, the supernatant was applied to a HisTrap column equilibrated with 20 mM HEPES, 0.5  
529 M NaCl, 5 mM imidazole, 6 M guanidine hydrochloride, 1 mM DTT pH 8. The equilibration buffer  
530 was then used to wash the column for a total of 5 CV followed by the same volume of 20 mM  
531 HEPES, 0.5 M NaCl, 20 mM imidazole, 6 M urea, 1 mM DTT pH 8. A linear gradient from the final  
532 wash buffer to 20 mM HEPES, 0.5 M NaCl, 20 mM imidazole, 0.1 mM CuSO<sub>4</sub>, 1 mM DTT pH 8 was  
533 then used to refold the tagged protein on the column. This was applied over 30 mL using a flow  
534 rate of 0.5 ml/min. To elute refolded protein another linear gradient was applied over 20 mL,  
535 starting with 20 mM HEPES, 0.3 M MgCl<sub>2</sub>, 20 mM imidazole, 1 mM DTT, pH 8 and ending with  
536 the same buffer with the addition of 500 mM imidazole and 10% glycerol. Apart from when  
537 otherwise mentioned, the flow rate was kept at 1 mL/ min when using a 1 mL capacity column  
538 and 3 mL/min when using a 5 mL capacity column. Fractions of 1.5 mL were collected  
539 throughout the elution step, and UV absorbance was used to determine protein content.  
540 Fractions with high protein contents were visualised using SDS–polyacrylamide gel  
541 electrophoresis (SDS-PAGE) and the presence of the recombinant protein confirmed through  
542 western blot analysis. Protein activity was confirmed through the measurement of 4MU from  
543 the GGβ4MU assay after removal of imidazole and DTT using Zeba™ Spin Desalting Columns, 7K  
544 MWCO (ThermoFisher) or Slide-A-Lyzer™ Dialysis Cassettes 10 K MWCO (ThermoFisher).

545 A second method to produce purified recombinant protein was also employed whereby cell  
546 pellets were suspended in 50 mL (50 mM Tris, 1 mM DTT, pH 8.5) and sonicated on ice. After  
547 centrifugation at 17,000 rpm for 45 min, supernatant was loaded onto an anion exchange  
548 chromatography mono-Q- HP column (5 mL, GE Healthcare) equilibrated with 50 mM Tris, 100

549 mm NaCl, 10% glycerol pH 8. The protein was then eluted with an increasing NaCl gradient (0 to  
550 1 M) over 100 mL. Fractions containing the protein of interest were pooled and concentrated  
551 using Millipore Vivaspin20 10kDa (Sartorius). These were then injected into a superdex 75  
552 (16/60) gel-filtration column (GE Healthcare) equilibrated with 50 mM Tris, 150 mM NaCl, 10%  
553 glycerol pH 8.5. SDS-PAGE was used to determine the purity of the eluted protein. Throughout  
554 the purification  $\beta$ -etherase activity was calculated (SI Appendix, Table S3). Concentration was  
555 calculated spectroscopically using the extinction coefficient at 280 nm.

#### 556 **Fluorescence assay for $\beta$ -etherase activity**

557 Enzyme activity was measured in 1 mL reaction containing 10  $\mu$ L 4MU/GG $\beta$ 4MU (synthetic  
558 fluorescent substrate 10 mM) and appropriate concentration of pure protein in 50 mM Tris-HCl,  
559 100 mM NaCl, pH 8.5, 5 mM CuSO<sub>4</sub>. The reaction was incubated at 30 °C for 1 h. Formation of 4-  
560 methylumbelliferone (4MU) was monitored using an RF-1500 fluorometric analyzer. After 0 h  
561 and 1 h of incubation 100  $\mu$ L of the reaction mixture was taken and added to 50  $\mu$ L of 100 mM  
562 glycine-NaOH buffer (pH 10.0). One unit of the enzyme was defined as the amount that released  
563 1 nmol of 4 MU/h from the substrate. Five replicates were taken for each sample, and control  
564 reactions of boiled enzyme and wheat straw treated with buffer only were also performed. The  
565 oxidative nature of the protein was investigated by performing this assay in an anaerobic  
566 chamber. All buffers were deoxygenated within the chamber overnight prior to experimental  
567 set-up. These assays were performed on pure protein.

#### 568 **Enzyme properties**

569 The effect of pH and temperature on enzyme activity was investigated on protein purified by  
570 anion-exchange and size-exclusion chromatography, by varying the pH of the reaction mixtures  
571 using 50 mM Tris-HCl buffer from pH 7.0 to 9.5, 50 mM glycine-NaOH buffer at pH range 9.0 to  
572 10.5 and 50 mM Na<sub>2</sub>HPO<sub>4</sub>-NaOH buffer at pH range 10.5 to 12. The optimum temperature of  
573 enzyme activity was determined at various temperatures ranging from 20 °C to 70 °C. Assays  
574 were performed as described in the previous section. Specificity was investigated by incubating  
575 1 mM of each substrate of interest with the enzyme in 100  $\mu$ L Tris pH 8.5 buffer at room  
576 temperature. Activity was determined by monitoring the change in Ultraviolet-Visible



577 absorbance spectra (220 - 750 nm) of aliquots using a NanoDrop 8000 Microvolume UV-Vis  
578 spectrophotometer (Thermo Scientific). Scans were performed at regular intervals over 2 h.

#### 579 **Extraction of tricin**

580 Wheat straw was ground to <1 mm using a cyclone mill (Retsch) and washed several times  
581 with 50 mM Tris pH 8 to remove surface sugars. In 1 mL reactions, 100 mg of washed wheat  
582 straw was incubated with purified enzyme in 50 mM Tris buffer at pH 8 with 5 mM CuSO<sub>4</sub>.  
583 Reactions were incubated overnight at 30 °C with shaking. Control reactions were performed  
584 using wheat straw incubated with buffer only. Tricin was extracted based upon the method  
585 described by Karambelkar (77). Briefly, 1 mL of ethyl acetate was added to 100 µL of the  
586 reaction supernatant. This was homogenized before being centrifuged for 5 min at 13,000 rpm.  
587 The ethyl acetate layer was transferred into new tubes and evaporated using a centrifugal  
588 evaporator at 55 °C before being resuspended in 100 µL 50% H<sub>2</sub>O, 50% acetonitrile. This was  
589 analyzed with a Waters 2996 photodiode array detector Separations Module HPLC system, with  
590 a C18-5 µM preparative column (4.6 × 250 mm, Waters). The mobile phase consisted of 0.1%  
591 acetic acid in H<sub>2</sub>O (A), and methanol (B). The following linear gradient was used; 95% A (5 min),  
592 70% A (25 min), 0% A (30 min), 95% A (5 min), the flow rate was 1.0 mL/min. After identification  
593 through comparisons with authentic standards, based on retention time and UV spectrum,  
594 peaks were manually collected and the mass confirmed with mass spectroscopy.

#### 595 **Oxidase activity boosting saccharification with cellulase enzymes**

596 For saccharification reactions, biomass pretreated with the oxidase was incubated with 1.2  
597 µg/mL enzyme cocktail (4:1 Celluclast: novo 188 (Novozymes)) in 50 mM sodium acetate at pH  
598 4.5 and incubated overnight at 37–40 °C with shaking. This was performed alongside a control  
599 reaction with buffer only. Solids were removed by centrifugation, and residual protein was  
600 precipitated with 80% ethanol. The supernatant, containing mono- and oligosaccharides, was  
601 dried with a centrifugal evaporator before samples were resuspended in ultra-pure water and  
602 filtered through a 0.2 µm polytetrafluoroethylene (PTFE) filter.

#### 603 **High-performance anion-exchange chromatography (HPAEC)**

604 HPAEC was used to analyze monosaccharide release after saccharification. Briefly, 5  $\mu$ L of  
605 samples or standards were injected on a CarboPac PA20 3  $\times$  150 mm analytical column via a  
606 CarboPac PA20 3 $\times$ 0 mm guard column using Chromeleon 6.8 Chromatography Data Systems  
607 software (Dionex). Sugars were separated at a flow rate of 0.4–0.5 mL min<sup>-1</sup> as follows: a linear  
608 gradient of 100% H<sub>2</sub>O to 99%–1% of H<sub>2</sub>O–0.2 M NaOH for 5 min, then constant for 10 min,  
609 followed by a 7 min linear gradient to 47.5%:22.5%:30% of H<sub>2</sub>O:0.2 M NaOH:0.5 M NaOAc/0.1 M  
610 NaOH then kept constant for 15 min. Between injections the column was washed with 0.2 M  
611 NaOH for 8 min and re-equilibrated with 100% H<sub>2</sub>O for 10 min. Carbohydrates were detected by  
612 ICS-3000 PAD system with an electrochemical gold electrode, identified by comparison with  
613 retention times of external standards, and quantified through the integration of those known  
614 standards.

#### 615 **Lignin isolation**

616 Enzyme lignins, representing essentially all of the lignin in the sample, were prepared following  
617 ball-milling of the cell wall isolate as previously described (56–58, 78).

#### 618 **NMR analysis**

619 2D NMR of enzyme lignins (EL) in 4:1 v/v DMSO-d<sub>6</sub>:pyridine-d<sub>5</sub> were acquired on a Bruker  
620 Biospin (Billerica, MA) Avance 700 MHz spectrometer equipped with a 5-mm <sup>1</sup>H/<sup>31</sup>P/<sup>13</sup>C/<sup>15</sup>N QCI  
621 cryoprobe with inverse geometry (proton coils closest to the sample), as described previously  
622 (57, 58). Volume-integration of contours in HSQC plots used TopSpin 4.07 (Mac version)  
623 software, and no correction factors were used. The data represent volume-integrals only, and  
624 data are presented on an S + G + H = 100% or an **A + B + C + C'** basis, although the latter are also  
625 provided on a 'number of linkages per 100 aromatic rings' basis also (Fig. 5); *p*CA, and triclin T  
626 units are always terminal and are, therefore, likely overestimated (58). Data assignments here  
627 were made by comparison with published data from other samples from our lab, including in  
628 the various triclin-related papers (7–10, 79, 80).

#### 629 **Statistical Analysis**

630 Where mentioned two tail ANOVAs were performed using R core package "stats" (81).

631 Differential gene analysis was performed using generalized linear models from R package

632 "edgeR".

### 633 **Data availability**

634 Metaproteomic and metatranscriptomic databases generated during this research are available

635 at MassIVE MSV000084758 and ProteomeXchange PXD016952. A curated dataset, which

636 includes annotations, is available in the Dataset S1. Amplicon sequences are deposited at the

637 European Nucleotide Archive under the accession PRJEB38167.

### 638 **Acknowledgments**

639

640 This work was funded by the Biotechnology and Biological Sciences Research Council (BBSRC),

641 UK (Grant BB/1018492/1 and BB/P027717/1), the BBSRC Network in Biotechnology and

642 Bioenergy LBNET. N.C.O and D.R.L. were supported by studentships from the BBSRC Doctoral

643 Training Programme (BB/J014443/1). A.A. acknowledges a Royal Society International Newton

644 Fellowship. J.R., S.L and V. T. acknowledge funding by the DOE Great Lakes Bioenergy Research

645 Center (DOE Office of Science, DE-SC0018409). The York Centre of Excellence in Mass

646 Spectrometry was created thanks to a major capital investment through Science City York,

647 supported by Yorkshire Forward with funds from the Northern Way Initiative, and subsequent

648 support from EPSRC (EP/ K039660/1; EP/M028127/1).

### 649 **References**

650

651 1. L. Caspeta, N. A. A. Buijs, J. Nielsen, The role of biofuels in the future energy supply. *Energy*  
652 *Environ. Sci.* **6**, 1077-1082 (2013).

653 2. J. V. Vermaas *et al.*, Mechanism of lignin inhibition of enzymatic biomass deconstruction.  
654 *Biotechnol. Biofuels* **8**, 16 (2015).

655 3. S.-Y. Ding *et al.*, How does plant cell wall nanoscale architecture correlate with enzymatic  
656 digestibility? *Science* **338**, 1055-1060 (2012).

657 4. Y. Ogo, K. Ozawa, T. Ishimaru, T. Murayama, F. Takaiwa, Transgenic rice seed synthesizing  
658 diverse flavonoids at high levels: a new platform for flavonoid production with associated  
659 health benefits. *Plant Biotechnol. J.* **11**, 734-746 (2013).

660 5. J. M. Duarte-Almeida, G. Negri, A. Salatino, J. E. de Carvalho, F. M. Lajolo, Antiproliferative  
661 and antioxidant activities of a tricin acylated glycoside from sugarcane (*Saccharum*  
662 *officinarum*) juice. *Phytochemistry* **68**, 1165-1171 (2007).

- 663 6. J. C. del Río *et al.*, Lignin monomers from beyond the canonical monolignol biosynthetic  
664 pathway: Another brick in the wall. *ACS Sustainable Chemistry & Engineering* **8**, 4997-  
665 5012 (2020).
- 666 7. J. C. del Río *et al.*, Structural characterization of wheat straw lignin as revealed by  
667 analytical pyrolysis, 2D-NMR, and reductive cleavage methods. *Journal of Agricultural and*  
668 *Food Chemistry* **60**, 5922-5935 (2012).
- 669 8. W. Lan *et al.*, Tricin-lignins: occurrence and quantitation of tricin in relation to phylogeny.  
670 *Plant J.* **88**, 1046-1057 (2016).
- 671 9. W. Lan *et al.*, Tricin, a flavonoid monomer in monocot lignification. *Plant Physiol.* **167**,  
672 1284-U1265 (2015).
- 673 10. W. Lan *et al.*, Maize tricin-oligolignol metabolites and their implications for monocot  
674 lignification. *Plant Physiol.* **171**, 810-820 (2016).
- 675 11. M. Li, Y. Pu, C. G. Yoo, A. Ragauskas, The occurrence of tricin and its derivatives in plants.  
676 *Green Chem.* **18** (2016).
- 677 12. G. M. Rashid *et al.*, Identification of manganese superoxide dismutase from  
678 *Sphingobacterium* sp. T2 as a novel bacterial enzyme for lignin oxidation. *ACS Chem. Biol.*  
679 **10**, 2286-2294 (2015).
- 680 13. K. Min, G. Gong, H. M. Woo, Y. Kim, Y. Um, A dye-decolorizing peroxidase from *Bacillus*  
681 *subtilis* exhibiting substrate-dependent optimum temperature for dyes and  $\beta$ -ether lignin  
682 dimer. *Sci. Rep.* **5**, 8245 (2015).
- 683 14. G. Janusz *et al.*, Lignin degradation: microorganisms, enzymes involved, genomes analysis  
684 and evolution. *FEMS Microbiol. Rev.* **41**, 941-962 (2017).
- 685 15. F. J. Ruiz-Dueñas, Á. T. Martínez, Microbial degradation of lignin: How a bulky recalcitrant  
686 polymer is efficiently recycled in nature and how we can take advantage of this. *Microb.*  
687 *Biotechnol.* **2**, 164-177 (2009).
- 688 16. Z. Duan, R. Shen, B. Liu, M. Yao, R. Jia, Comprehensive investigation of a dye-decolorizing  
689 peroxidase and a manganese peroxidase from *Irpex lacteus* F17, a lignin-degrading  
690 basidiomycete. *AMB Express* **8**, 119 (2018).
- 691 17. B. Goodell *et al.*, Modification of the nanostructure of lignocellulose cell walls via a non-  
692 enzymatic lignocellulose deconstruction system in brown rot wood-decay fungi.  
693 *Biotechnol. Biofuels* **10**, 179 (2017).
- 694 18. B. Goodell *et al.*, Low molecular weight chelators and phenolic compounds isolated from  
695 wood decay fungi and their role in the fungal biodegradation of wood. *J. Biotechnol.* **53**,  
696 133-162 (1997).
- 697 19. V. Arantes, B. Goodell, *Current understanding of brown-rot fungal biodegradation*  
698 *mechanisms: A review*, Deterioration and Protection of Sustainable Biomaterials  
699 (American Chemical Society, 2014), vol. 1158, pp. 3-21.
- 700 20. R. Cohen, M. R. Suzuki, K. E. Hammel, Processive endoglucanase active in crystalline  
701 cellulose hydrolysis by the brown rot basidiomycete *Gloeophyllum trabeum*. *Appl.*  
702 *Microbiol. Biotechnol.* **71**, 2412-2417 (2005).
- 703 21. D. J. Yelle, J. Ralph, F. Lu, K. E. Hammel, Evidence for cleavage of lignin by a brown rot  
704 basidiomycete. *Environ. Microbiol.* **10**, 1844-1849 (2008).
- 705 22. F. Barras, F. Van Gijsegem, A. K. Chatterjee, Extracellular enzymes and pathogenesis of  
706 soft-rot *Erwinia*. *Annu. Rev. Phytopathol.* **32**, 201-234 (2003).
- 707 23. G. van Erven *et al.*, Evidence for ligninolytic activity of the ascomycete fungus *Podospora*  
708 *anserina*. *Biotechnol. Biofuels* **13**, 75 (2020).

- 709 24. U. Kõljalg *et al.*, UNITE: a database providing web-based methods for the molecular  
710 identification of ectomycorrhizal fungi. *New Phytol.* **166**, 1063-1068 (2005).
- 711 25. K. Abarenkov *et al.*, The UNITE database for molecular identification of fungi – recent  
712 updates and future perspectives. *New Phytol.* **186**, 281-285 (2010).
- 713 26. A. M. Alessi *et al.*, Defining functional diversity for lignocellulose degradation in a  
714 microbial community using multi-omics studies. *Biotechnol. Biofuels* **11**, 166 (2018).
- 715 27. A. M. Alessi *et al.*, Revealing the insoluble metasecretome of lignocellulose-degrading  
716 microbial communities. *Sci. Rep.* **7**, 2356 (2017).
- 717 28. H. Jun, H. Guangye, C. Daiwen, Insights into enzyme secretion by filamentous fungi:  
718 Comparative proteome analysis of *Trichoderma reesei* grown on different carbon sources.  
719 *J. Proteomics* **89**, 191-201 (2013).
- 720 29. N. L. Glass, M. Schmoll, J. H. D. Cate, S. Coradetti, Plant cell wall deconstruction by  
721 ascomycete fungi. *Annu. Rev. Microbiol.* **67**, 477-498 (2013).
- 722 30. D. M. de Oliveira *et al.*, Ferulic acid: a key component in grass lignocellulose recalcitrance  
723 to hydrolysis. *Plant Biotechnol. J.* **13**, 1224-1232 (2015).
- 724 31. J. Zhang, M. Siika-Aho, M. Tenkanen, L. Viikari, The role of acetyl xylan esterase in the  
725 solubilization of xylan and enzymatic hydrolysis of wheat straw and giant reed. *Biotechnol.*  
726 *Biofuels* **4**, 60 (2011).
- 727 32. A. Levasseur, E. Drula, V. Lombard, P. M. Coutinho, B. Henrissat, Expansion of the  
728 enzymatic repertoire of the CAZy database to integrate auxiliary redox enzymes.  
729 *Biotechnol. Biofuels* **6**, 41 (2013).
- 730 33. G. Vaaje-Kolstad *et al.*, An oxidative enzyme boosting the enzymatic conversion of  
731 recalcitrant polysaccharides. *Science* **330**, 219-222 (2010).
- 732 34. R. J. Quinlan *et al.*, Insights into the oxidative degradation of cellulose by a copper  
733 metalloenzyme that exploits biomass components. *PNAS* **108**, 15079-15084 (2011).
- 734 35. C. Laurent, E. Breslmayr, D. Tunega, R. Ludwig, C. Oostenbrink, Interaction between  
735 cellobiose dehydrogenase and lytic polysaccharide monooxygenase. *Biochemistry* **58**,  
736 1226-1235 (2019).
- 737 36. T.-C. Tan *et al.*, Structural basis for cellobiose dehydrogenase action during oxidative  
738 cellulose degradation. *Nat. Commun.* **6**, 7542 (2015).
- 739 37. L. Munk, A. K. Sitarz, D. C. Kalyani, J. D. Mikkelsen, A. S. Meyer, Can laccases catalyze bond  
740 cleavage in lignin? *Biotechnology Advances* **33**, 13-24 (2015).
- 741 38. R. Hilgers, J.-P. Vincken, H. Gruppen, M. A. Kabel, Laccase/Mediator Systems: Their  
742 Reactivity toward Phenolic Lignin Structures. *ACS Sustainable Chemistry & Engineering* **6**,  
743 2037-2046 (2018).
- 744 39. A. Levasseur *et al.*, Exploring laccase-like multicopper oxidase genes from the ascomycete  
745 *Trichoderma reesei*: a functional, phylogenetic and evolutionary study. *BMC Biochemistry*  
746 **11** (2010).
- 747 40. P. Kersten, D. Cullen, Extracellular oxidative systems of the lignin-degrading  
748 basidiomycete *Phanerochaete chrysosporium*. *Fungal Genet. Biol.* **44**, 77-87 (2007).
- 749 41. P. Daly *et al.*, Expression of *Aspergillus niger* CAZymes is determined by compositional  
750 changes in wheat straw generated by hydrothermal or ionic liquid pretreatments.  
751 *Biotechnol. Biofuels* **10**, 35 (2017).
- 752 42. W. Schutyser *et al.*, Chemicals from lignin: an interplay of lignocellulose fractionation,  
753 depolymerisation, and upgrading. *Chem. Soc. Rev.* **47**, 852-908 (2018).

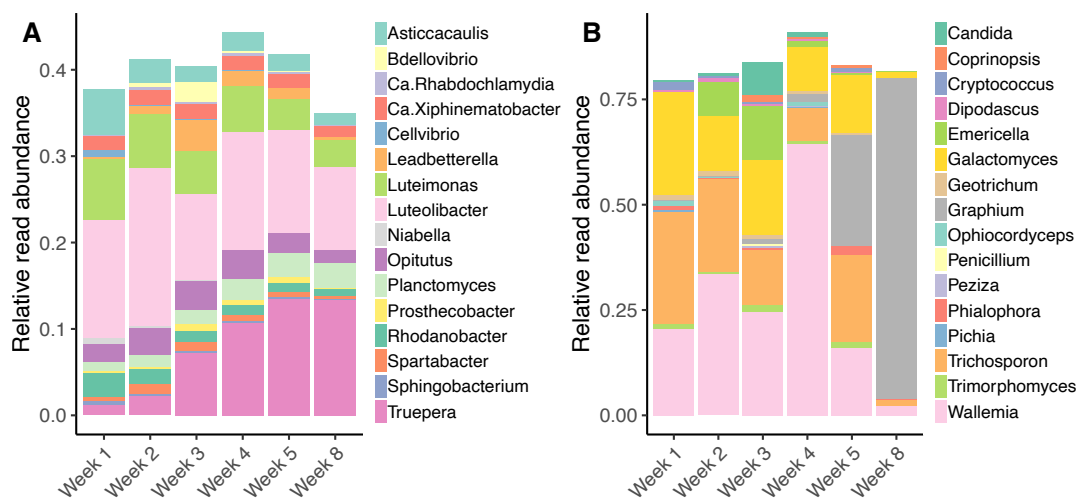
- 754 43. D. L. Gall *et al.*, *In vitro* enzymatic depolymerization of lignin with release of syringyl,  
755 guaiacyl, and triclin units. *Appl. Environ. Microbiol.* **84**, e02076-02017 (2018).
- 756 44. W. S. Kontur *et al.*, A heterodimeric glutathione S-transferase that stereospecifically  
757 breaks lignin's  $\beta$ (R)-aryl ether bond reveals the diversity of bacterial  $\beta$ -etherases. *J. Biol.*  
758 *Chem.* **294**, 1877-1890 (2019).
- 759 45. M. Marinović *et al.*, Selective cleavage of lignin  $\beta$ -O-4 aryl ether bond by  $\beta$ -etherase of the  
760 white-rot fungus *Dichomitus squalens*. *ACS Sustainable Chemistry & Engineering* **6**, 2878-  
761 2882 (2018).
- 762 46. Y. Otsuka *et al.*, Detection and characterization of a novel extracellular fungal enzyme that  
763 catalyzes the specific and hydrolytic cleavage of lignin guaiacylglycerol  $\beta$ -aryl ether  
764 linkages. *Eur. J. Biochem.* **270**, 2353-2362 (2003).
- 765 47. D. A. Weinstein, M. H. Gold, Synthesis of guaiacylglycol and glycerol- $\beta$ -O-( $\beta$ -  
766 methylumbelliferyl) ethers: lignin model substrates for the possible fluorometric assay of  
767  $\beta$ -etherases. *Holzforschung* **33**, 134-135 (1979).
- 768 48. R. D. Finn *et al.*, The Pfam protein families database. *Nucleic Acids Res.* **38**, D211-D222  
769 (2010).
- 770 49. M. Kanteev, M. Goldfeder, A. Fishman, Structure-function correlations in tyrosinases.  
771 *Protein Sci.* **24**, 1360-1369 (2015).
- 772 50. K. Min *et al.*, Perspectives for biocatalytic lignin utilization: cleaving 4-O-5 and C $\alpha$ -C $\beta$   
773 bonds in dimeric lignin model compounds catalyzed by a promiscuous activity of  
774 tyrosinase. *Biotechnol. Biofuels* **10**, 212 (2017).
- 775 51. S. Halaoui, M. Asther, J. C. Sigoillot, M. Hamdi, A. Lomascolo, Fungal tyrosinases: new  
776 prospects in molecular characteristics, bioengineering and biotechnological applications.  
777 *J. Appl. Microbiol.* **100**, 219-232 (2006).
- 778 52. N. Hakulinen, C. Gasparetti, H. Kaljunen, K. Kruus, J. Rouvinen, The crystal structure of an  
779 extracellular catechol oxidase from the ascomycete fungus *Aspergillus oryzae*. *J. Biol.*  
780 *Inorg. Chem.* **18**, 917-929 (2013).
- 781 53. C. Gasparetti *et al.*, Discovery of a new tyrosinase-like enzyme family lacking a C-  
782 terminally processed domain: production and characterization of an *Aspergillus oryzae*  
783 catechol oxidase. *Applied Microbiology and Biotechnology* **86**, 213-226 (2010).
- 784 54. Z. Yang, D. A. Robb, Comparison of tyrosinase activity and stability in aqueous and nearly  
785 nonaqueous environments. *Enzyme Microb. Technol.* **15**, 1030-1036 (1993).
- 786 55. S. Zolghadri *et al.*, A comprehensive review on tyrosinase inhibitors. *J. Enzyme Inhib.* **34**,  
787 279-309 (2019).
- 788 56. H.-M. Chang, E. B. Cowling, W. Brown, E. Adler, G. Miksche, Comparative studies on  
789 cellulolytic enzyme lignin and milled wood lignin of sweetgum and spruce. *Holzforschung*  
790 **29**, 153-159 (1975).
- 791 57. H. Kim, J. Ralph, Solution-state 2D NMR of ball-milled plant cell wall gels in DMSO-  
792  $d_6$ /pyridine- $d_5$ . *Org. Biomol. Chem.* **8**, 576-591 (2010).
- 793 58. S. D. Mansfield, H. Kim, F. Lu, J. Ralph, Whole plant cell wall characterization using  
794 solution-state 2D-NMR. *Nature protocols* **7**, 1579-1589 (2012).
- 795 59. Y. Mu, L. Li, S.-Q. Hu, Molecular inhibitory mechanism of triclin on tyrosinase. *Spectrochim.*  
796 *Acta A Mol. Biomol. Spectrosc.* **107**, 235-240 (2013).
- 797 60. J. Y. Lim, K. Ishiguro, I. Kubo, Tyrosinase inhibitory *p*-coumaric acid from ginseng leaves.  
798 *Phytother. Res.* **13**, 371-375 (1999).

- 799 61. G. van Erven *et al.*, Mechanistic insight in the selective delignification of wheat straw by  
800 three white-rot fungal species through quantitative <sup>13</sup>C-IS py-GC-MS and whole cell wall  
801 HSQC NMR. *Biotechnol. Biofuels* **11**, 262 (2018).
- 802 62. S. Hutner, L. Provasoli, A. Schatz, C. Haskins, Some approaches to the study of the role of  
803 metals in the metabolism of microorganisms. *Proceedings of the American Philosophical*  
804 *Society* **94**, 152-170 (1950).
- 805 63. White, T. Bruns, S. Lee, J. Taylor, "Amplification and direct sequencing of fungal ribosomal  
806 RNA genes for phylogenetics" in PCR Protocols: A guide to methods and applications.  
807 (1990), pp. 315-322.
- 808 64. A. Klindworth *et al.*, Evaluation of general 16S ribosomal RNA gene PCR primers for  
809 classical and next-generation sequencing-based diversity studies. *Nucleic Acids Res* **41**, e1  
810 (2013).
- 811 65. J. G. Caporaso *et al.*, QIIME allows analysis of high-throughput community sequencing  
812 data. *Nature methods* **7**, 335-336 (2010).
- 813 66. D. McDonald *et al.*, An improved Greengenes taxonomy with explicit ranks for ecological  
814 and evolutionary analyses of bacteria and archaea. *ISME* **6**, 610-618 (2012).
- 815 67. T. Z. DeSantis *et al.*, Greengenes, a chimera-checked 16S rRNA gene database and  
816 workbench compatible with ARB. *Appl. Environ. Microbiol.* **72**, 5069-5072 (2006).
- 817 68. K. Abarenkov *et al.*, The UNITE database for molecular identification of fungi-recent  
818 updates and future perspectives. *New Phytol.* **186**, 281-285 (2010).
- 819 69. M. A. Bezerra, R. E. Santelli, E. P. Oliveira, L. S. Villar, L. A. Escaleira, Response surface  
820 methodology (RSM) as a tool for optimization in analytical chemistry. *Talanta* **76**, 965-977  
821 (2008).
- 822 70. N. C. Oates, "Mining microbial compost communities for lignocellulose degrading  
823 proteins", University of York, York, U.K, (2016).
- 824 71. M. Lever, Colorimetric and fluorometric carbohydrate determination with *p*-  
825 hydroxybenzoic acid hydrazide. *Biochemical Medicine* **7**, 274-281 (1973).
- 826 72. H. Zhang *et al.*, dbCAN2: a meta server for automated carbohydrate-active enzyme  
827 annotation. *Nucleic Acids Res.* **46**, W95-W101 (2018).
- 828 73. R. D. Finn, J. Clements, S. R. Eddy, HMMER web server: interactive sequence similarity  
829 searching. *Nucleic Acids Res.* **39**, W29-W37 (2011).
- 830 74. C. Camacho *et al.*, BLAST+: architecture and applications. *BMC Bioinformatics* **10**, 421  
831 (2009).
- 832 75. T. N. Petersen, S. Brunak, G. von Heijne, H. Nielsen, SignalP 4.0: discriminating signal  
833 peptides from transmembrane regions. *Nature methods* **8**, 785-786 (2011).
- 834 76. Y. Ishihama *et al.*, Exponentially modified protein abundance index (emPAI) for estimation  
835 of absolute protein amount in proteomics by the number of sequenced peptides per  
836 protein. *Mol. Cell. Proteomics* **4**, 1265-1272 (2005).
- 837 77. P. Karambelkar, Jadhav, V.M. , Kadam, V., Isolation and characterization of flavonoid tricin  
838 from sugarcane sludge. *Indo American Journal of Pharmaceutical Research* **4**, 7 (2014).
- 839 78. H. Kim *et al.*, Monolignol benzoates incorporate into the lignin of transgenic *Populus*  
840 *trichocarpa* depleted in C3H and C4H. *ACS Sustainable Chemistry & Engineering* **8**, 3644-  
841 3654 (2020).
- 842 79. J. Rencoret *et al.*, Structural characterization of lignin isolated from coconut (*Cocos*  
843 *nucifera*) Coir Fibers. *J. Agric. Food Chem.* **61**, 2434-2445 (2013).

- 844 80. W. Lan *et al.*, Elucidating tricin-lignin structures: Assigning correlations in HSQC spectra of  
845 monocot lignins. *Polymers (Basel)* **10**, 916 (2018).
- 846 81. R. C. Team (2019) R: A Language and Environment for Statistical Computing. (Vienna,  
847 Austria).
- 848
- 849

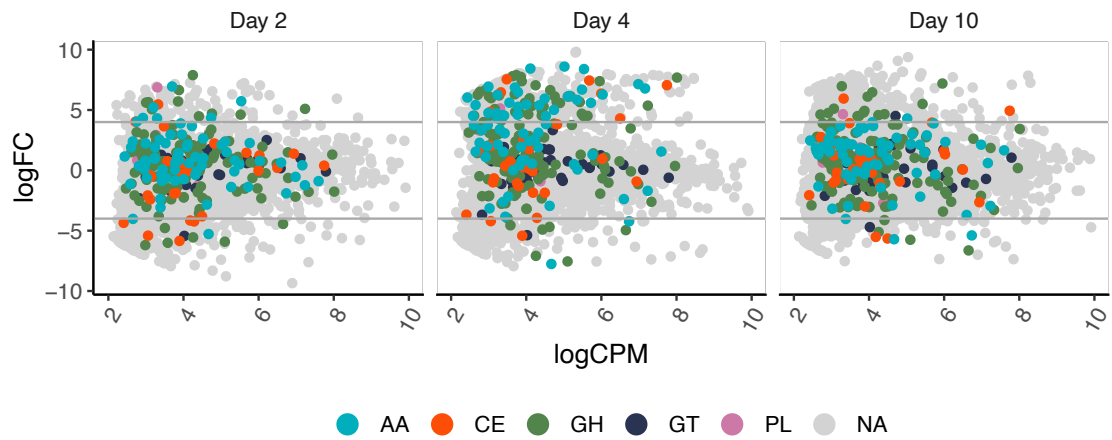


850 **Figures and Tables**  
 851



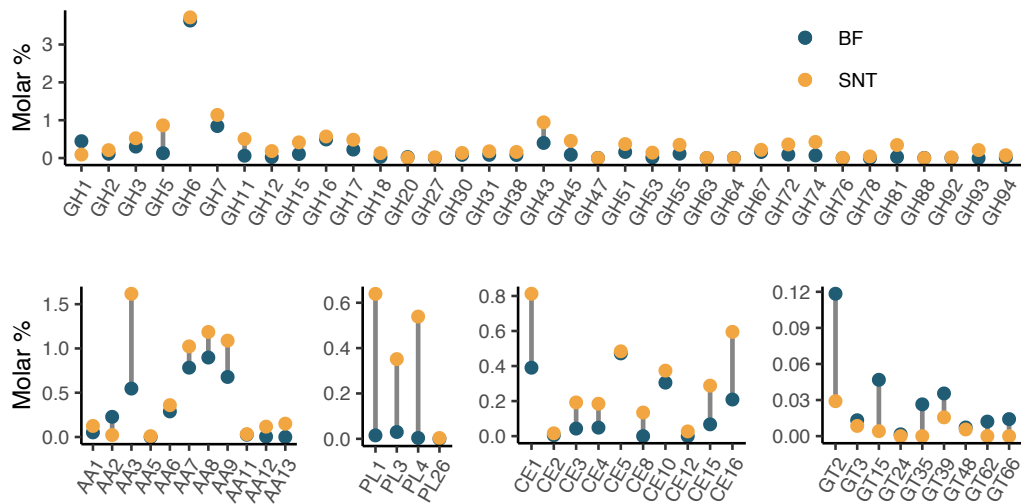
852  
 853  
 854  
 855  
 856  
 857  
 858  
 859  
 860  
 861  
 862  
 863

**Figure 1.** Composition of prokaryotic and fungal genera during wheat straw degradation. Sequences were generated on an ion torrent platform after amplification of the 16S and ITS for (A) prokaryotic and (B) eukaryotic identification, respectively. Operational taxonomic units were identified to genus level N=1.



864  
865  
866  
867  
868  
869  
870  
871  
872  
873  
874

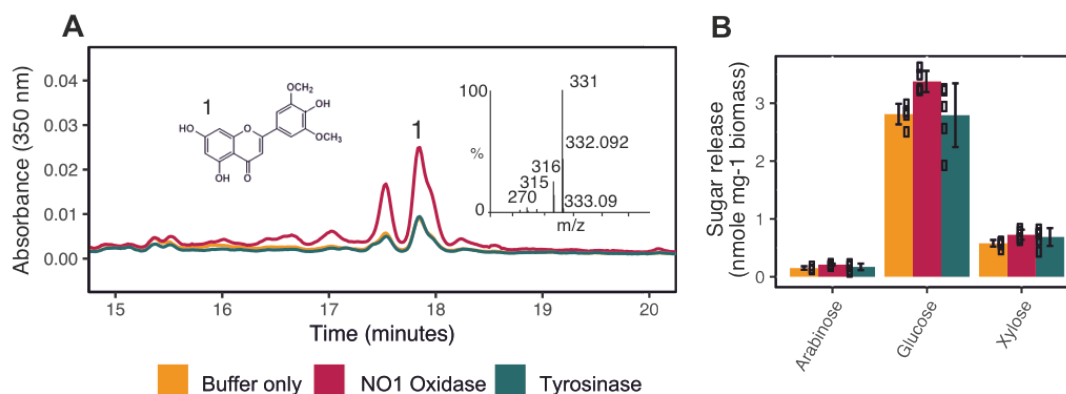
**Figure 2.** Expression change of contigs between glucose and wheat straw conditions. RNA was extracted and sequenced after two, four and ten days of *P. putredinis* NO1 incubation on wheat straw and four days of growth on glucose. Points represent the log fold change (FC) and average counts per million (CPM) of contigs, between the wheat straw and glucose conditions. Carbohydrate-active enzymes were annotated using dbCAN namely auxiliary activities (AA), glycoside hydrolases (GH), polysaccharide lyases (PL), carbohydrate esterases (CE) and glycosyltransferases (GT). Points are the average of three biological replicates.



875  
876  
877  
878  
879  
880  
881  
882

**Figure 3.** Molar percentages of supernatant (SNT) and biotin-labelled (BF) proteins after four days of incubation on wheat straw. Molar percentages of carbohydrate-active families, GH: Glycoside hydrolase, AA: Auxiliary activity, PL: Polysaccharide lyase, CE: Carbohydrate esterase and GT Glycosyl transferase, were calculated as the sum of contigs annotated and taken as an average for each biological replicate.

883



884

885

886

887

888

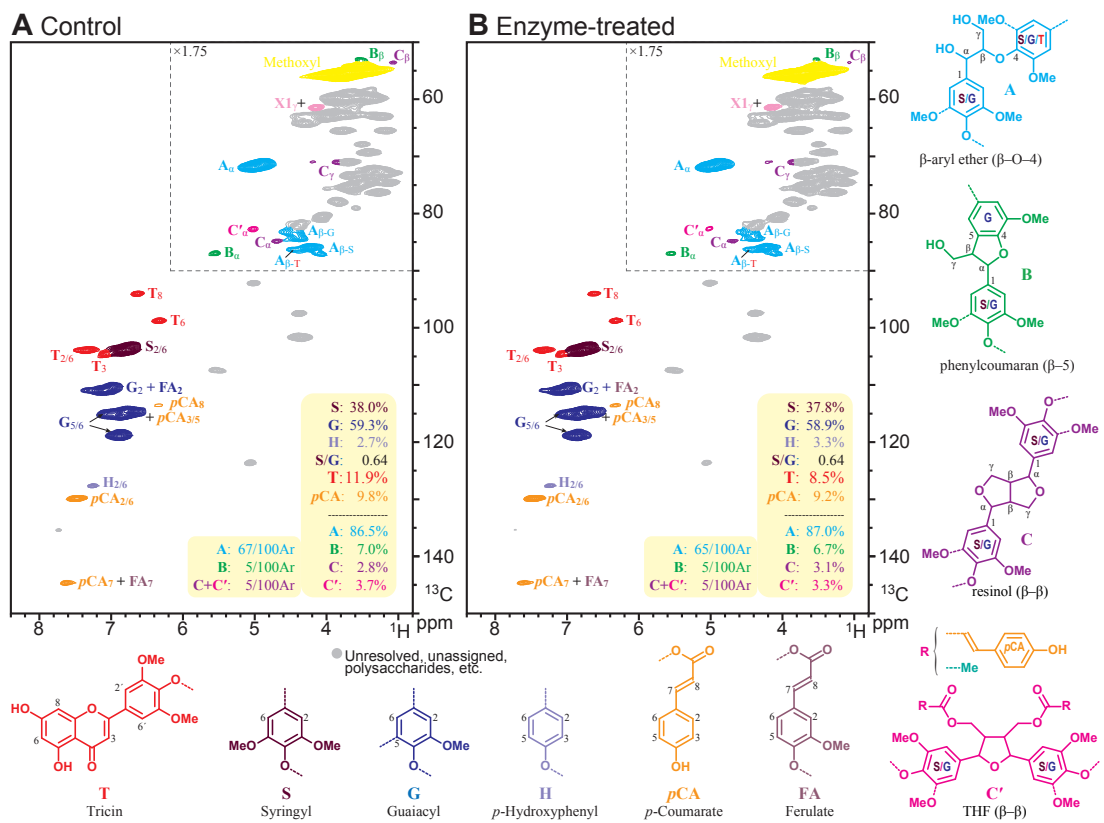
889

890

891

892

**Figure 4.** Treatment of Biomass with recombinant oxidase. (A) Tricin 1 release from wheat straw was observed and compared to an authentic standard using a High-Performance Liquid-Chromatography (HPLC), and mass was confirmed by time-of-flight mass spectrometry. (B) wheat straw was treated with recombinant oxidase, commercial mushroom tyrosinase, and buffer only for 16 h prior to the application of Celluclast® commercial saccharification cocktail. Sugar release was calculated from the reaction mixture using High-Performance Anion-Exchange chromatography. Error bars represent the standard deviation of five biological replicates.



893

894 **Figure 5.** Lignin aromatic and side-chain region of 2D HSQC NMR spectra (DMSO- $d_6$ :pyridine- $d_5$ ,  
 895 4:1, v/v) of enzyme lignins (EL) from (A) the wheat control, and (B) the enzyme-treated wheat.  
 896 The quantification values in the yellow boxes are for relative comparisons of the lignin  
 897 components determined from NMR contour volume-integrals based on **S + G + H = 100%** or an **A**  
 898 **+ B + C + C'** basis, although the latter are also provided on a 'number of linkages per 100  
 899 aromatic rings' basis also. The **pCA** and **T** units are lignin appendages; their levels were  
 900 estimated and expressed based on the total lignin (**S + G + H**). The chemical structures of the  
 901 lignin monomeric subunits are color-coded to match their signal assignments in the spectra.  
 902 Assignments are from papers noted in the Experimental Section, along with the new  $A_{\beta-T}$   
 903 assignment (80). Note that, to allow the crucial lignin side-chain contours to be more clearly  
 904 seen, the boxed lignin side-chain region was vertically scaled by  $\sim 1.75\times$ .



Supplementary information for

A multi-omics approach to lignocellulolytic enzyme discovery: uncovering a new ligninase activity from *Parascedosporium putredinis* NO1

Nicola C. Oates<sup>1</sup>, Amira Abood<sup>1</sup>, Alexandra M. Schirmacher<sup>1</sup>, Anna M. Alessi<sup>1</sup>, Susannah M. Bird<sup>1</sup>, Joseph P. Bennett<sup>1</sup>, Daniel R. Leadbeater<sup>1</sup>, Yi Li<sup>1</sup>, Adam A. Dowle<sup>2</sup>, Vitaliy I. Tymokhin<sup>3</sup>, John Ralph<sup>3</sup>, Simon J. McQueen-Mason<sup>1</sup>, Neil C. Bruce<sup>1</sup>

<sup>1</sup>Centre for Novel Agricultural Products, Department of Biology, University of York, York, YO10 5DD, UK.

<sup>2</sup>Bioscience Technology Facility, Department of Biology, University of York, York, YO10 5DD, UK.

<sup>3</sup>Department of Biochemistry, University of Wisconsin-Madison, Madison, WI, 53706, USA

Correspondence and requests for materials should be addressed to N.C.B.

Email: neil.bruce@york.ac.uk

**This PDF file includes:**

Figures S1 to S12

Table S1 to S4

**Other supplementary materials for this manuscript include the following:**

Dataset S1

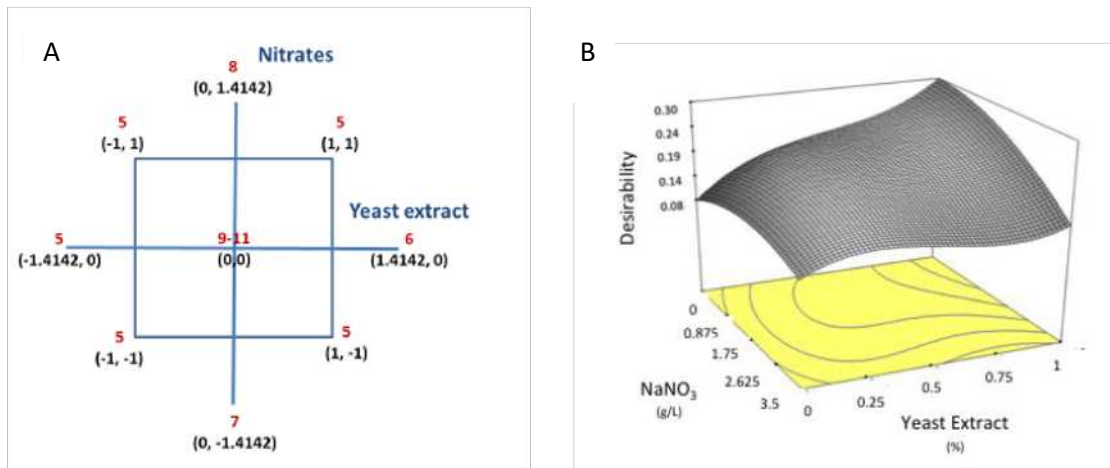


**Fig. S1.** Optimisation of *P. putredinis* NO1 growth media. (A) central composite design was used to create a response surface morphology to yeast extract and sodium nitrate concentrations. (B) Both cellulase and xylanase production was improved with a high yeast extract and low nitrate concentrations.

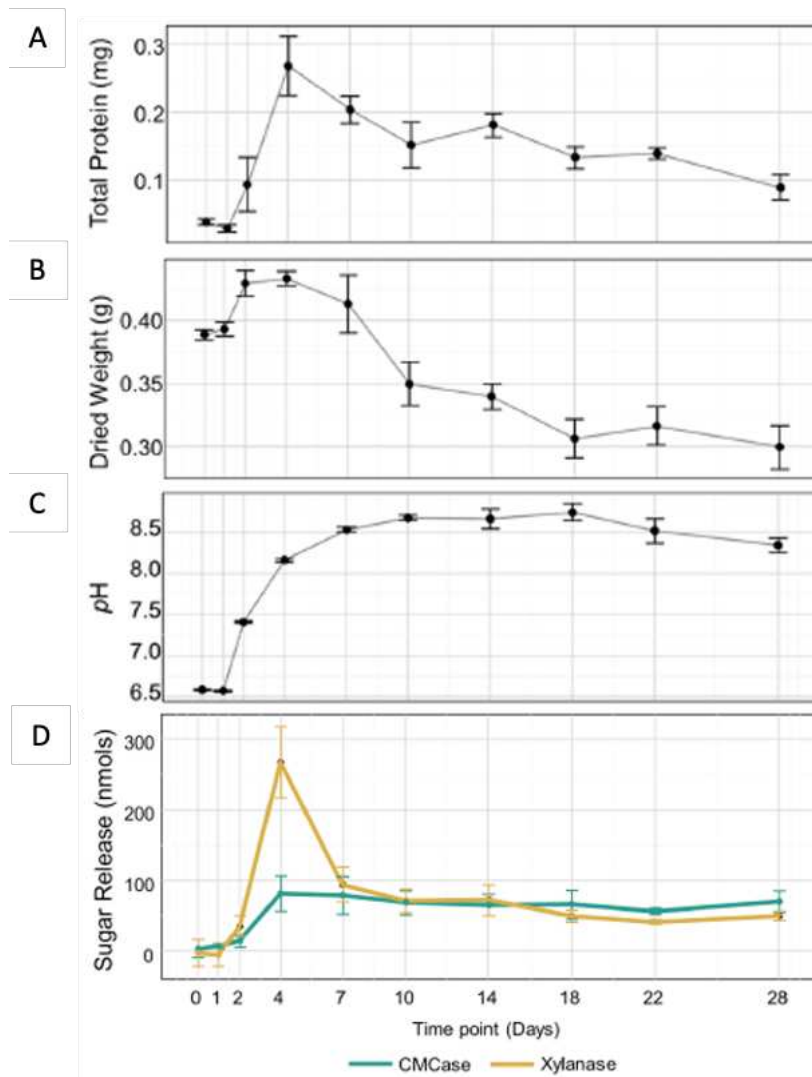


**Fig. S2.** Growth of *P. putredinis* NO1 on wheat straw over a period of one month. Growth of *P. putredinis* NO1 on wheat straw estimated by (A) the total protein present in the culture and (B) the dried weight of the total biomass within the culture. (C) The pH of the culture was also monitored alongside (D) the release of sugar after 1 h from 10 % supernatant loading on carboxymethylcellulose and beechwood xylan.



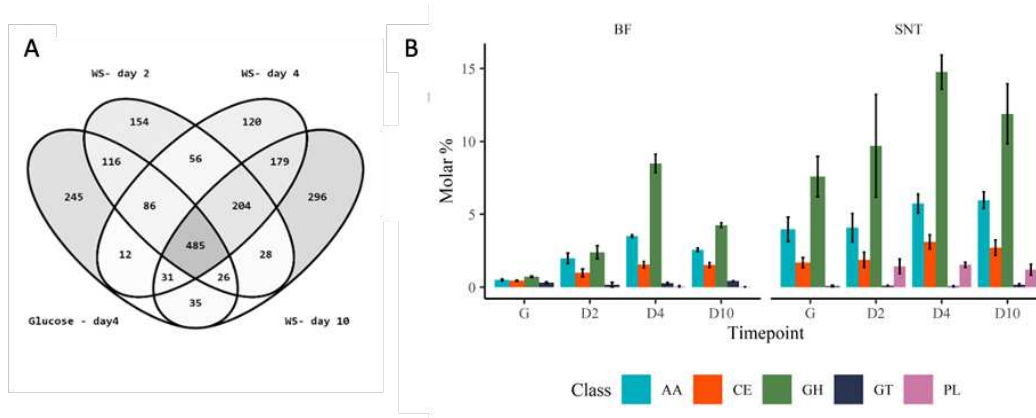


**Fig. S3.** Proteomics of *P. putredinis* NO1 grown on wheat straw. (A) Total proteins recovered from *P. putredinis* NO1 exoproteome across timepoints. (B) Total molar percentage of CAZy class across timepoints in the biotin labelled protein sample and supernatant.

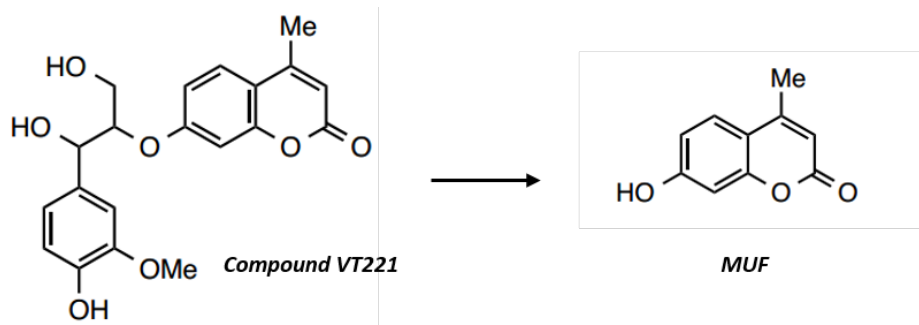


**Fig. S4.** GGβ4MU β-etherase assay. Under the action of a β-etherase the 4-O-β-ether linkage is cleaved liberating the product MUF. Upon excitement at 372 nm MUF will fluoresce at 445 nm.

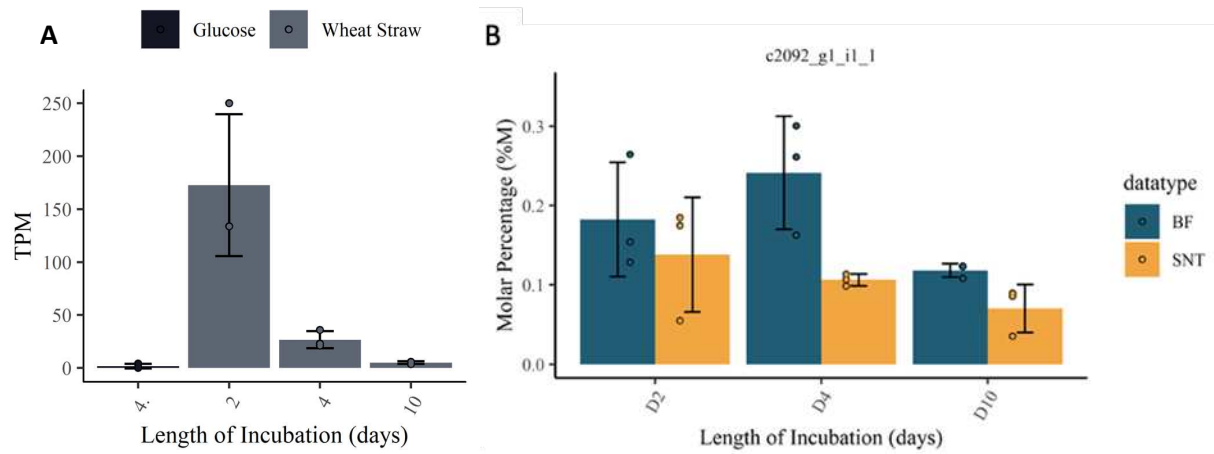


**Fig. S5.** c2092\_g1\_i1 abundance within the transcriptomic and proteomic libraries. (A) Transcript per million (TPM) of c2092\_g1\_i1 after growth on wheat straw and glucose and (B) molar percent abundance. Circles represent sample values of biological replicates (N=3), and error bars  $\pm$  SD of the mean.

2Y9W	-----	0
2P3X	-----APIQAPDISKCGTATVPDGVTP-TNCCPPV	29
c2092	-MPSAKRLGLLLAATAAVGVAAQEPALTEDDFSIPEI-----EGGDALAQLAQLAADS	53
4J3P	MVALQALSGLLLASQALAFPAASQAAA-----TATLPTTASSTAVASSQLDQLANFAYNV	56
1WX2	-----	0
4J6V	-----	0
2Y9W	-----SDKKSMLPLVGIPEIKNRRLNILDVFNKDKFFTLVVRALQVLQARDQSDYSSFF	54
2P3X	T-----TKIIDFQLPSSGSPMRTRPAHLVSKE--YLAKYKKAIEIQALPDDDRSFK	81
c2092	SQETALRMAKRGNSGCSQIKVRRWRTLTSA--QRKQYIASVKCLQTKPSFFDPNII	111
4J3P	TT-DSVAGGSESKRGGCTLQNLVRRDRWRAFSKT--QKKDYINSVLCLQKLPSTRPAHLA	113
1WX2	-----MTVRKNQATLTAD--EKRRFVAAVLELKR-----	27
4J6V	-----MGNKYVRKKNVHLHLDLTD--EKRFVVRTVLILKE-----	31
	* . : : :	
2Y9W	QLGGIHGL---PYTEWA---KAQPQ---LHLYKANYCTGTVLFPTWFRAYESTWEQTLW	105
2P3X	QQANVHCTYCQGAIDQVGYTD-----LELQVHASWFLPFHRYLYFNERILA	129
c2092	P-----AAKSLFDDFVGVVVFQ-----TGSILTLATFLTWERYFVYTYETKLR	154
4J3P	P-----GARTRYDDFVATINIQ-----TQIINHTGTFLAWERYFYEFQALR	156
1WX2	-----SGRYDEFVRTINEFIMS--DTDSGERTGRSPSFLPWRFRLLDFEQALQ	75
4J6V	-----KGIYDRYIAWHGAAGKFHTPPGSDRNAAMSSAFLPWRREYLLRFERDLQ	81
:	* : * : * : * * *	
2Y9W	EAAGTVAQRFTTSDQAEWIAQAAKDLRQPFWDWGYWPNDP----DFIGLDPQVIRDKQVE-	160
2P3X	KLI-----DDPTFALPYAWNDNPDGMYPMT-IYASSPSSLYDEKRNA-	170
c2092	E-E-----CGYTGPLPYEWGLDVNNPNASPVFDGSDTSLSGNGAFF-	195
4J3P	D-E-----CSYTGDPYWNWGDADNMEKSQVFDGSETSMSGNGEYI-	197
1WX2	S-V-----D-SSVTLPYWDWSADRTV----RASLWAPDFLGGTGRSTD	112
4J6V	S-I-----N-PEVTLPLYWEWETDAQMQDPSQSQIWSADFMGGNGNPIK	122
.	* : * * *	
2Y9W	-----ITDYNGTKI-----EVENPI--LHYKFHPIEPTFEGDFAQW--QT	196
2P3X	-----KHLPTTV-----IDLDDYDGTPTIPDDELKTD---	197
c2092	---AHEGIQMVQPIINGNILKLPNGGGCVTKGPFKDMKVHFGTIIIPVYQPIILSGVEN	252
4J3P	---PNQGDIKLLGNYPALDLPFGSGGGCVTSKPFKDYKLNLPAAALSPPGGNM-TAAAN	253
1WX2	GRVM-DGPFAASTGNWPIN-VRVDSRTY-----LRRSLGG---SVAELPTRAEVES	158
4J6V	DFIVDTGPFVAA--GRWTTIDEQGNPSGG-----LKRNFVATK-EAFTLPTTRDDVNL	170
2Y9W	TMRY-PDVQKQENIEGMIAGIKAAAPGFREWTFNMLTKNYTWELFSNHGAVVGAHANSL	255
2P3X	---NLAIMYKQ-----IVSGATTPKFLG-YPYRAGD-----AIDPGAGTLEH	236
c2092	PIADNERCLKRD---LNAGIAKRFTSFLNSTS-VILKNNNIEMFQAHLQGGDDRYVNLNL	307
4J3P	PLTYNPRCMKRS---LTTEILQRYNTFPKIVE-LILDSDDIWFQMTMQGVPG--SGSI	306
1WX2	VLA-----ISAYDLP-----PYNAS-EGFRNHLEGW-----RGV	187
4J6V	ALK-----ITQYDTP-----PWDMTSQNSFRNQLGEGF----INGP	201
2Y9W	MVNTVFLIGRDPDLDPLVPGHMG-SVPHAAFDFIFWMCNVDRLALWQTMNYDVYV	314
2P3X	APHNIVKWTGLAD---KPSDMG-NFYTAGRDPFFGHANVDRMWNWIKTIGGKNRK	291
c2092	GVGGGTYTIG-----GDPGGDPFISPGDPAFYLHAQIDRIYWIWQMLDFKNRQ	357
4J3P	GVGGGYSMG-----GDPGRDYYVSPGDTAFWLHGMDRVDVWVWQNLDRKRQ	356
1WX2	NLNRVWVWG-----GQMA-T-GVSPNDPVFWLHAYVDKLWAEWQRRHPDSAY	235
4J6V	QLDRVLRVVG-----GQMG-VVPTAPNDPVFFLHANVDRIWAVWQIIHRNQNY	250
	* . * . : * * : * * : * : * :	
2Y9W	SEGMNREATMGLIPGQVLTEDSLEP----FYTKNQDPWQSDDLEDWETLGFSPDFDPV	370
2P3X	DF-----T-----DTDWLDATFVFDENKQL-----VKV	315
c2092	G-----V-----HGTA---TLQN---NPPSANVTVE--D--TIDLSP-APPV	389
4J3P	NA-----I-----SGTG---TFMN---NPASPNTLD--T--VIDLGYANGGPI	390
1WX2	VP-----T-----GGTP---DVVDLN-ETMKPWNTV-----RP-	259
4J6V	QP-----M-----KNGP---FGQNFR-DPMYPWNTT-----PE-	274
.		
2Y9W	KGKSK----EEKSVYIND----WVHKHYG----	391
2P3X	KVSDCV---DTSKLRYYQDIPIPWLP-----	339
c2092	KIKDLMNTVGGSPLCYIYL-----	408
4J3P	AMRDLMSTT-AGPFCYVYL-----	408
1WX2	---ADLL---DHTAYYTFDALEHHHHHH-----	281
4J6V	---DVMN---HRKLGYYVDIELRKSRSRSHHHHHH	303

**Fig. S6.** Alignment of the putative  $\beta$ -etherase amino acid sequence (c2092\_g1\_i1) with structurally related enzymes. Alignment with 2Y9W; tyrosinase from *Agaricus bisporus* (common mushroom), 2P3X; *Vitis vinifera* Polyphenol Oxidase, 4J3P; catechol oxidase *Aspergillus oryzae*, 1WX2; *Streptomyces castaneoglobisporus* tyrosinase, 4J6V; *Bacillus megaterium* N205D tyrosinase. Identical amino acids are indicated by asterisks and amino acids similarity by dots. The conserved N-terminal arginine residue is highlighted with a red box; copper-binding regions are in green.

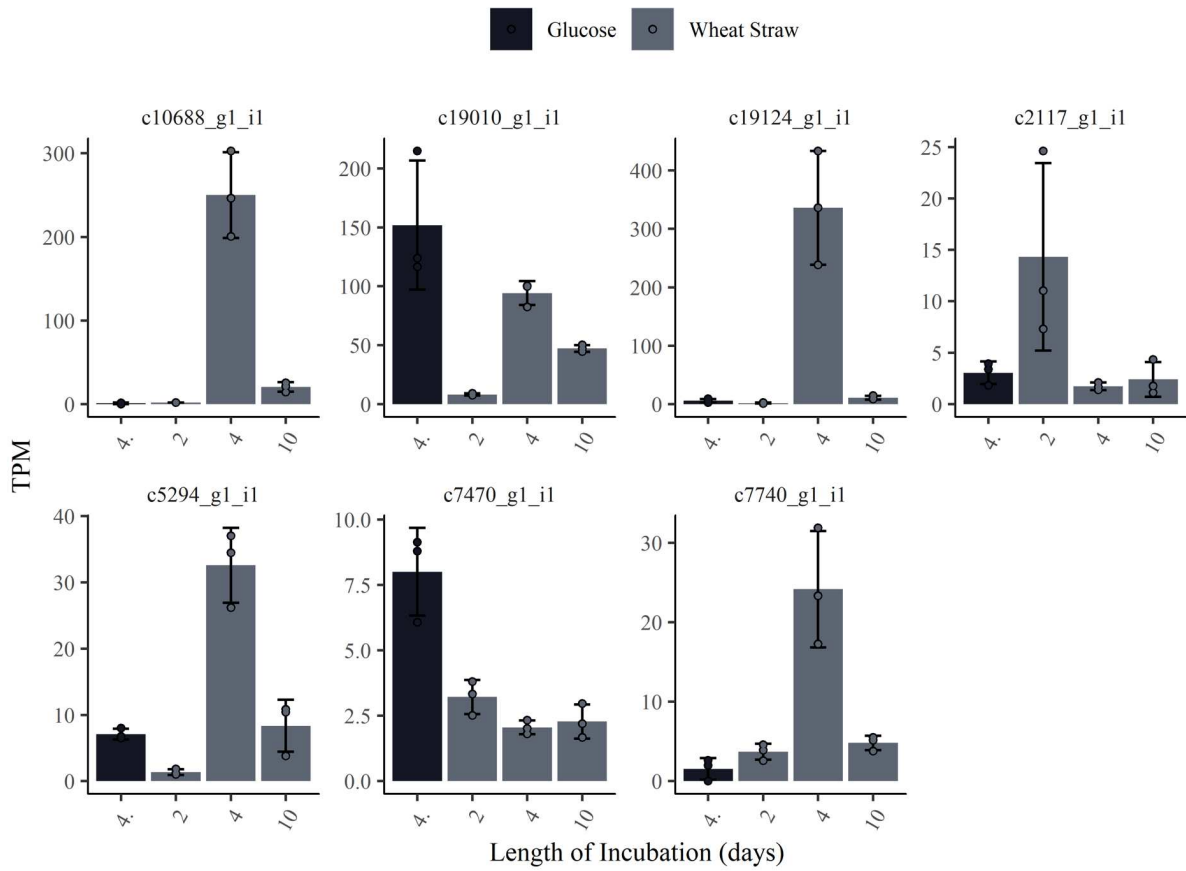


**Fig. S7.** Transcript per million (TPM) of contigs identified as sharing significant similarity with c2092\_g1\_i1. Reads with a similarity identity of over 30 % to c2092\_g1\_i1 were considered as displaying significant homology. Circles represent sample values of biological replicates (N=3), and error bars  $\pm$  SD of the mean.

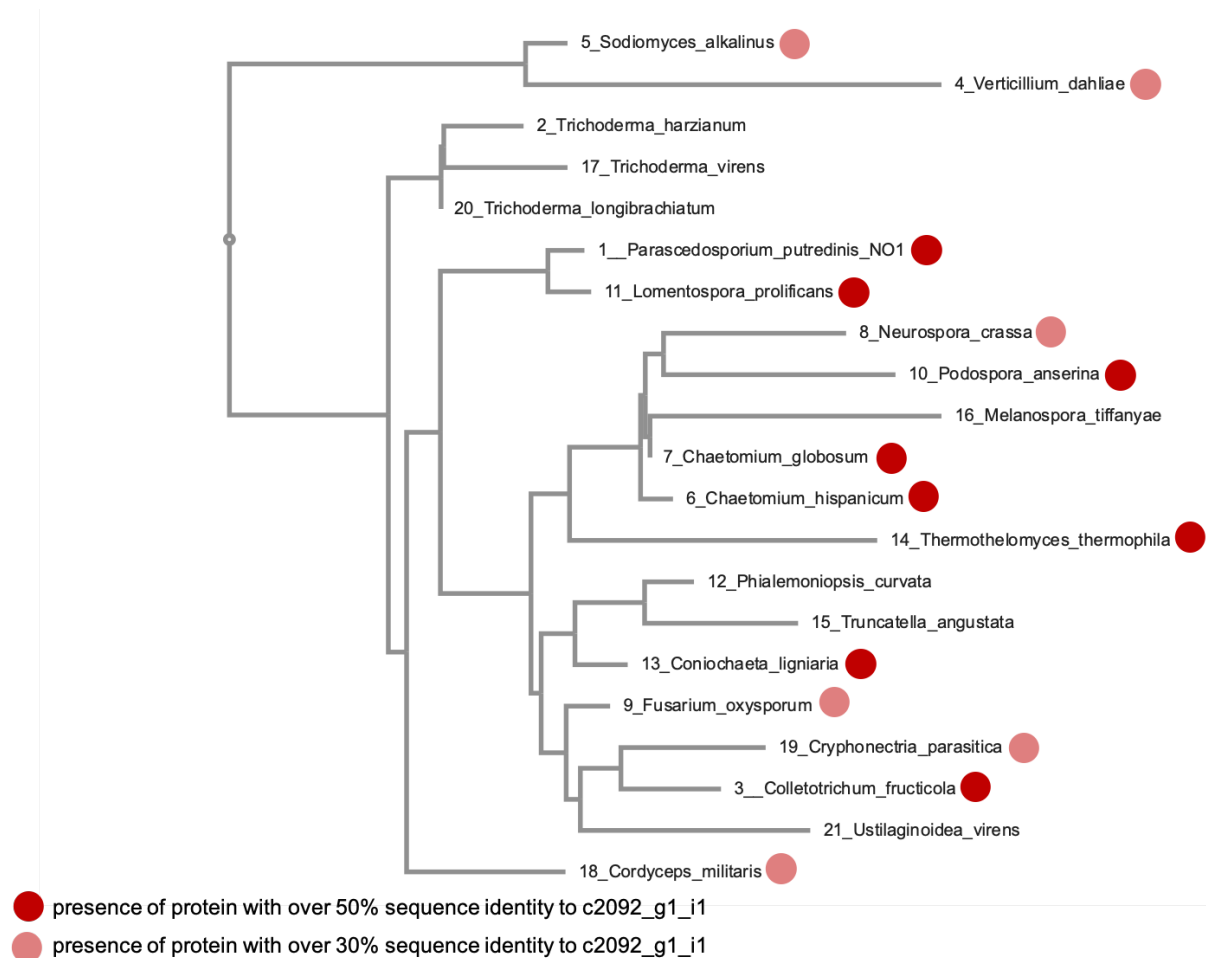


**Fig. S8.** Distribution of proteins with over 30 % identity to c2092\_g1\_i1 amongst species from the Sordariomycetes class. The phylogenetic tree was assembled from ITS sequences downloaded from the UNITE database. Multiple sequence alignment was performed using MAFFT (<https://mafft.cbrc.jp>). The phylogenetic tree was assembled using neighbor joining on conserved sites, and the Jukes-Cantor substitution model was used.

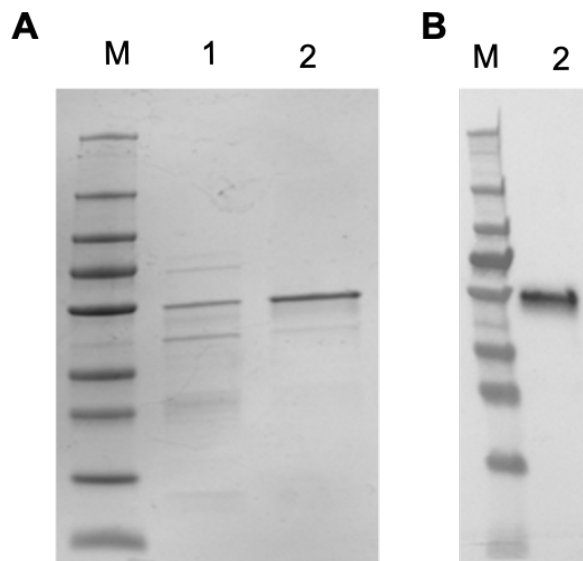


**Fig. S9.** Identification of the recombinant protein by SDS-PAGE (A) and western blot analysis (B). Lane M: molecular weight standards (PageRuler Plus Thermo Scientific). 1: denatured protein purified and refolded in the absence of CuSO<sub>4</sub>, 2: denatured protein refolded in the presence of 0.1 mM CuSO<sub>4</sub>. Protein identity was confirmed through western blotting using Anti-6-His antibody (B) and mass-spectrometry.

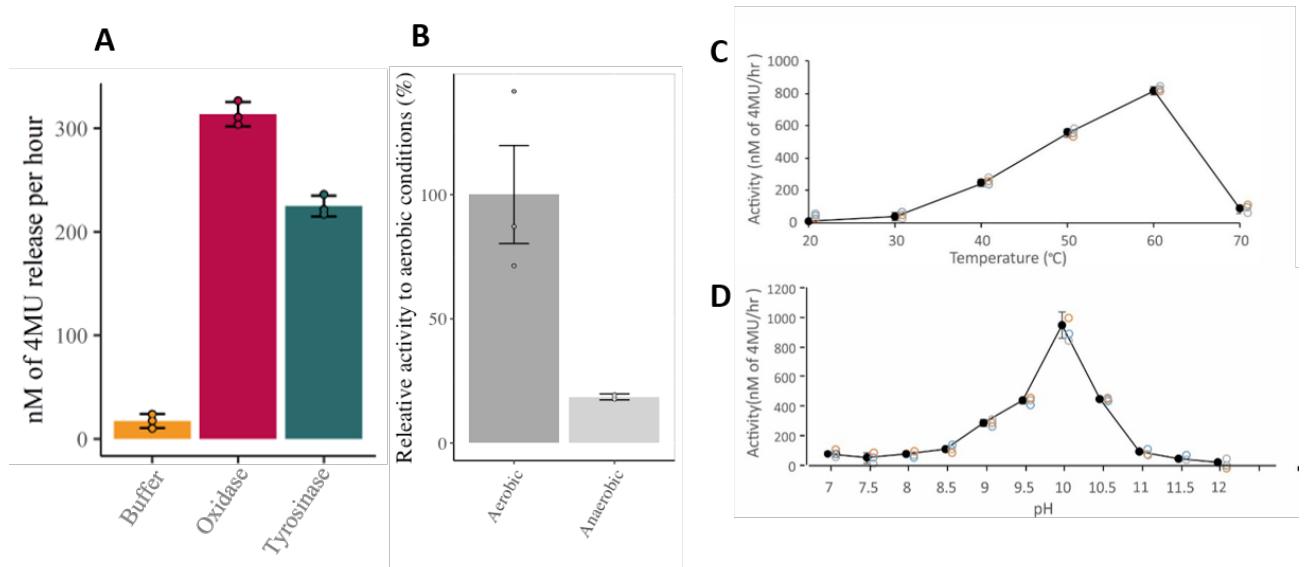


**Fig. S10.**  $\beta$ -etherase activity of the oxidase against the synthetic substrate GG $\beta$ 4MU. (A) Fluorescence activity of purified protein against commercial mushroom tyrosinase and buffer control reaction. (B) GG $\beta$ 4MU assay performed in presence and absence of oxygen with recombinant protein (C-D) optimum temperature and pH as assessed by GG $\beta$ 4MU assay. Circles represent sample values, and bars sample mean  $\pm$  SD, N=3.



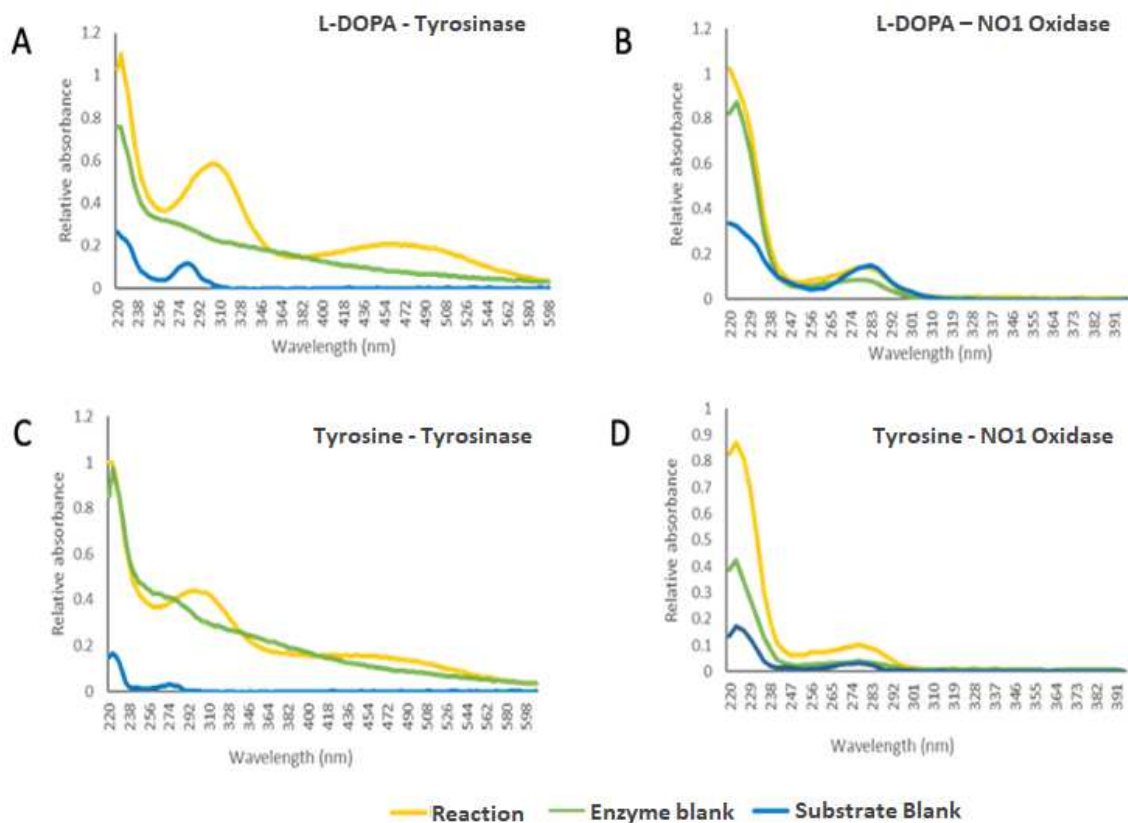


**Fig. S11.** UV spectra showing activity of the *P. putredinis* NO1 oxidase and tyrosinase against different phenolic compounds. Either was incubated in 50mM Tris pH 8.5 at room temperature with 1mM of substrate against enzyme only or substrate only as controls, (A) L-DOPA reaction with tyrosinase, (B) L-DOPA reaction with the oxidase, (C) tyrosine reaction with tyrosinase, (D) tyrosine reaction with the oxidase.

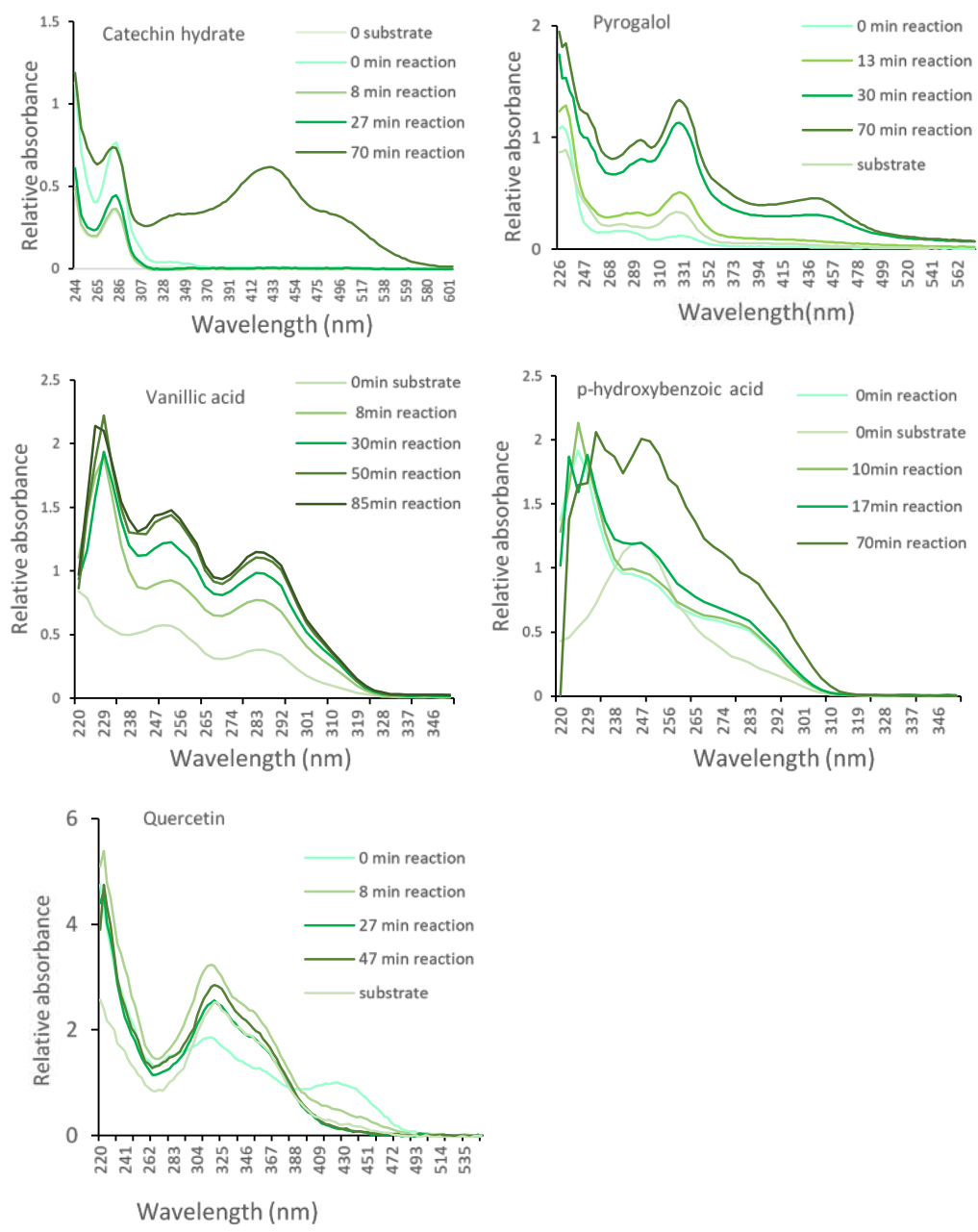


**Fig. S12.** UV spectra showing activity of the *P. putredinis* NO1 oxidase against different phenolic compounds. 1mg/mL of the enzyme was incubated in 50mM Tris pH 8.5 at room temperature with 1mM of either catechin hydrate, pyrogallol, vanillic acid, p-hydroxybenzoic acid or quercetin.

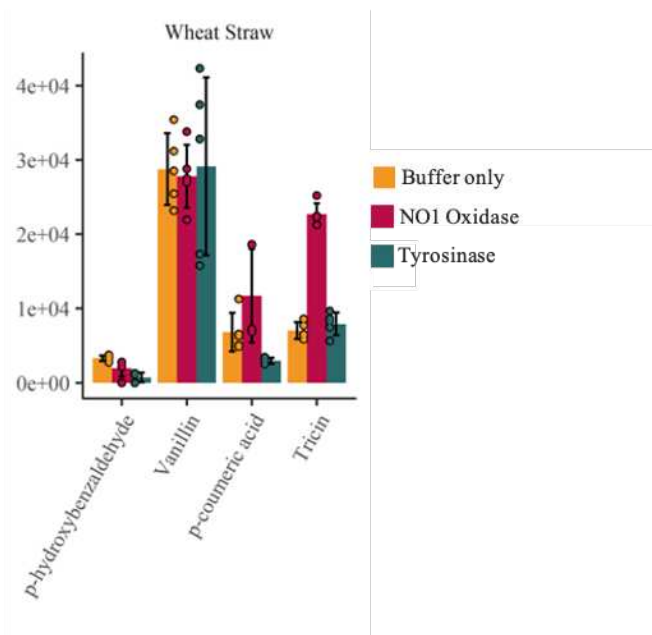


**Fig. S13.** Release of products from lignocellulosic substrates after incubation with NO1 oxidase, mushroom tyrosinase and buffer only. Reactions were performed at physiological pH 8.5 and 30 °C prior to the reaction products being extracted from the reaction supernatant using ethyl acetate and analysed with high-performance liquid-chromatography. Circles represent the individual sample values (N=5), and error bars  $\pm$  SD of the mean.

**Table S1.** Proteins showing homology to the oxidase within the transcriptome of *P. putredinis* NO1. BLASTp searches were performed on the c2092\_g1\_i1 sequence against the assembled *P. putredinis* NO1 transcriptome.

<b>sseqid</b>	<b>evalue</b>	<b>pident</b>	<b>length</b>	<b>bitscore</b>	<b>Similarity%</b>	<b>Similarity</b>
<b>c19124_g1_i1_4</b>	9.4E-111	43.796	411	330	0.608	256/421
<b>c7740_g1_i1_6</b>	8.17E-77	38.482	382	243	0.508	23/439
<b>c10688_g1_i1_2</b>	1.72E-74	40.395	354	236	0.52	226/435
<b>c5294_g1_i1_3</b>	1.65E-71	37.366	372	229	0.52	223/429
<b>c2117_g1_i1_2</b>	2.9E-57	36.963	349	191	0.422	184/436
<b>c19010_g1_i1_4</b>	2.94E-32	29.254	335	125	0.325	164/505
<b>c7470_g1_i1_2</b>	2.25E-26	23.37	368	108	0.376	169/449

**Table S2.** Proteins with homology to the oxidase within NCBI non-redundant database. BLASTp searches were performed on the c2092\_g1\_i1 sequence against the non-redundant protein database held by NCBI. Results were filtered to >50 % identity.

	Description	Max Score	Total Score	Query Cover	E value	Percent identity
gb PKS12997.1	hypothetical protein jhhlp_000338 [Lomentospora prolificans]	713	713	100%	0.0	87.50%
ref XP_016642676.1	Tyrosinase central domain protein [Scedosporium apiospermum]	674	674	100%	0.0	82.40%
gb TPX10091.1	hypothetical protein EOL32_001288 [Phialemoniopsis curvata]	572	572	93%	0.0	67.19%
gb ELA32929.1	tyrosinase central domain protein [Colletotrichum fructicola Nara qc5]	506	506	99%	7e-176	57.95%
gb KZL67883.1	tyrosinase central domain-containing protein [Colletotrichum tofieldiae]	501	501	97%	8e-174	58.90%
gb EQB58959.1	hypothetical protein CGLO_00722 [Colletotrichum gloeosporioides Cg-14]	497	497	92%	3e-172	59.89%
gb KZL82263.1	tyrosinase central domain-containing protein [Colletotrichum incanum]	496	496	97%	3e-172	58.15%
gb KXH49404.1	tyrosinase central domain-containing protein [Colletotrichum nymphaeae SA-01]	486	486	99%	2e-168	55.88%
gb KXH35131.1	tyrosinase central domain-containing protein [Colletotrichum simmondsii]	485	485	99%	1e-167	55.64%
gb OLN85731.1	Grixazone synthase 2 [Colletotrichum chlorophyti]	484	484	92%	3e-167	58.99%
ref XP_018157362.1	Tyrosinase central domain-containing protein [Colletotrichum higginsianum IMI 349063]	481	481	92%	4e-166	59.37%
gb EXF76797.1	tyrosinase central domain-containing protein [Colletotrichum fiorinae PJ7]	479	479	99%	2e-165	55.15%
gb TDZ75107.1	Tyrosinase-like protein orsC [Colletotrichum trifolii]	476	476	92%	4e-164	59.95%
gb TKW48599.1	hypothetical protein CTA1_467 [Colletotrichum tanacetii]	473	473	92%	7e-163	58.42%
gb TDZ15437.1	Tyrosinase-like protein orsC [Colletotrichum orbiculare MAFF 240422]	470	470	92%	4e-162	60.48%
ref XP_001227696.1	hypothetical protein CHGG_09769 [Chaetomium globosum CBS 148.51]	469	469	100%	2e-161	55.50%
gb TDZ29471.1	Tyrosinase-like protein orsC [Colletotrichum spinosum]	460	460	92%	2e-157	57.00%
ref XP_022470530.1	tyrosinase central domain-containing protein [Colletotrichum orchidophilum]	458	458	99%	2e-157	54.66%
gb OIW32989.1	tyrosinase central domain-containing protein [Coniochaeta ligniaria NRRL 30616]	447	447	92%	5e-153	53.79%

gb KXH30586.1	<u>tyrosinase central domain-containing protein</u> [ <u>Colletotrichum salicis</u> ]	447	447	97%	3e-152	54.02%
gb RKU41032.1	<u>hypothetical protein DL546_002981</u> [ <u>Coniochaeta pulveracea</u> ]	442	442	99%	5e-151	51.96%
gb KZL64229.1	<u>tyrosinase central domain-containing protein</u> [ <u>Colletotrichum incanum</u> ]	434	434	92%	4e-145	55.17%
gb TEA15757.1	<u>Tyrosinase-like protein orsC</u> [ <u>Colletotrichum sidae</u> ]	427	427	92%	6e-145	55.00%
gb OHW92206.1	<u>tyrosinase central domain-containing protein</u> [ <u>Colletotrichum incanum</u> ]	420	420	84%	5e-143	57.73%
ref XP_018162984.1	<u>Tyrosinase central domain-containing protein</u> [ <u>Colletotrichum higginsianum</u> IMI 349063]	425	425	92%	1e-142	54.38%
gb TID02585.1	<u>Tyrosinase ustQ</u> [ <u>Colletotrichum higginsianum</u> ]	425	425	92%	1e-142	54.38%
gb OLN83361.1	<u>Tyrosinase 2</u> [Colletotrichum chlorophyti]	417	417	92%	5e-141	51.97%
emb CCF32411.1	<u>hypothetical protein CH063_04807</u> [ <u>Colletotrichum higginsianum</u> ]	412	412	84%	7e-140	56.85%
gb KZL72889.1	<u>tyrosinase-like protein</u> [ <u>Colletotrichum tofieldiae</u> ]	412	412	84%	7e-140	57.14%
gb TKW50870.1	<u>hypothetical protein CTA1_3684</u> [Colletotrichum tanacetii]	419	419	92%	7e-140	52.39%
gb KDN70624.1	<u>hypothetical protein CSUB01_04485</u> [ <u>Colletotrichum sublineola</u> ]	417	417	92%	1e-139	53.58%
gb EXF84421.1	<u>hypothetical protein CFIO01_02736</u> [ <u>Colletotrichum fioriniae</u> PJ7]	409	409	92%	1e-136	52.22%
ref XP_003664995.1	<u>tyrosinase-like protein</u> [ <u>Thermothelomyces thermophilus</u> ATCC 42464]	404	404	92%	3e-136	54.09%
gb TQN72542.1	<u>Tyrosinase-like protein orsC</u> [ <u>Colletotrichum</u> sp. PG-2018a]	407	407	89%	5e-136	54.77%
ref XP_003351009.1	<u>uncharacterized protein SMAC_04313</u> [Sordaria macrospora k-hell]	399	399	97%	6e-134	50.12%
ref XP_006692366.1	<u>hypothetical protein CHTH_0018720</u> [ <u>Chaetomium thermophilum</u> var. <u>thermophilum</u> DSM 1495]	395	395	89%	1e-132	54.67%
gb TDZ58291.1	<u>Tyrosinase-like protein orsC</u> [ <u>Colletotrichum trifolii</u> ]	393	393	79%	6e-132	57.67%
gb TDZ23501.1	<u>Nitroalkane oxidase</u> [ <u>Colletotrichum orbiculare</u> MAFF 240422]	409	409	80%	8e-132	57.75%
ref XP_022471338.1	<u>hypothetical protein CORC01_10513</u> [ <u>Colletotrichum orchidophilum</u> ]	397	397	92%	9e-132	50.78%
gb KXH34366.1	<u>hypothetical protein CSIM01_00277</u> [ <u>Colletotrichum simmondsii</u> ]	396	396	92%	2e-131	50.51%

gb KXH69104.1	<u>hypothetical protein</u> CSAL01_01466 [ <u>Colletotrichum salicis</u> ]	389	389	81%	3e-129	56.19%
ref XP_008090963.1	<u>hypothetical protein</u> GLRG_02114 [ <u>Colletotrichum graminicola</u> M1.001]	378	378	79%	2e-126	56.44%
ref XP_001227853.1	<u>hypothetical protein</u> CHGG_09926 [Chaetomium globosum CBS 148.51]	373	373	92%	5e-124	50.00%
gb TDZ28941.1	<u>Tyrosinase-like protein orsC</u> [ <u>Colletotrichum spinosum</u> ]	371	371	73%	2e-122	58.14%
gb ELA37064.1	<u>hypothetical protein</u> CGGC5_3508 [ <u>Colletotrichum fructicola</u> Nara gc5]	364	364	72%	1e-121	59.52%
ref XP_007911158.1	<u>putative tyrosinase-like</u> <u>protein</u> [Phaeoacremonium minimum UCRPA7]	363	363	68%	2e-121	59.22%
gb EQB52888.1	<u>hypothetical protein</u> CGLO_07432 [ <u>Colletotrichum</u> <u>gloeosporioides Cg-14</u> ]	361	361	72%	2e-120	59.86%
gb TEA10724.1	<u>Nitroalkane oxidase</u> [ <u>Colletotrichum sidae</u> ]	373	373	73%	4e-118	58.33%
ref XP_024731024.1	<u>putative tyrosinase</u> [ <u>Meliniomyces bicolor E</u> ]	331	331	79%	2e-108	51.38%
emb CDP29730.1	<u>Putative tyrosinase</u> [ <u>Podospora anserina S</u> <u>mat+</u> ]	326	326	81%	4e-106	50.15%
emb VBB81548.1	<u>Putative tyrosinase</u> [ <u>Podospora comata</u> ]	326	326	81%	5e-106	50.15%
ref XP_001273822.1	<u>tyrosinase, putative</u> [ <u>Aspergillus clavatus NRRL</u> <u>1</u> ]	326	326	83%	2e-105	50.00%
ref XP_001905273.1	<u>uncharacterized protein</u> PODANS_5_7480 [ <u>Podospora anserina S</u> <u>mat+</u> ]	323	323	80%	3e-105	50.00%
gb PGH18781.1	<u>hypothetical protein</u> AJ79_00194 [Helicocarpus griseus UAMH5409]	325	325	83%	5e-105	50.15%
gb PBP21500.1	<u>hypothetical protein</u> BUE80_DR007716 [ <u>Diplocarpon rosae</u> ]	278	278	68%	4e-88	50.17%

**Table S3.** Purification of recombinant protein. The heterologously expressed protein was purified using anion exchange (Q) and size-exclusion chromatography (S.E). Protein concentration and VT221 activity was calculated after each purification step.

<b>Purification steps</b>	<b>Total Protein mg</b>	<b>Activity(mU) (nmol/mg/hr)</b>	<b>Specific (U/mg)</b>	<b>Yield (%)</b>	<b>Purification fold</b>
<b>Culture filtrate</b>	1024	7500	7.32	100	1
<b>Q</b>	29.25	2600	88	34.67	12
<b>S.E</b>	14	1950	139	26	19



**Table S4.** Substrate specificity of the *P. putredinis* NO1 oxidase.

<b>Substrate</b>	<b>Etherase reactivity</b>	<b>Tyrosinase reactivity</b>
<b>Tyrosine methyl ester</b>	-	+
<b>L-Dopa(3,4-dihydroxy-L-phenylalanine)</b>	-	+
<b>Dopamine hydrochloride</b>	-	+
<b>Caffeic acid (catechol oxidase substrate)</b>	-	+
<b>4-Methyl-Catechol (catechol oxidase substrate)</b>	-	+
<b>Tyrosol (catechol oxidase substrate)</b>	-	-
<b>Tannic acid</b>	-	-
<b>(+)-catechin hydrate</b>	+	+
<b>Pyrogallol</b>	+	+
<b>4-hydroxybenzoic acid</b>	+	-
<b>Quercetin</b>	+	-
<b>Vanillic acid</b>	+	-

**Dataset S1 (separate file).**

Descriptions of sequences containing catalytic carbohydrate active domains.